MORPHOLOGY ENGINEERING AND CATALYTIC STUDIES OF CuO NANOPARTICLES DERIVED FROM COORDINATION POLYMERS

Harikrishnan R
MS15057

A dissertation submitted for the partial fulfilment of
BS-MS dual degree in Science

Indian Institute of Science Education and Research Mohali

June 2020

DEDICATED to
MY PARENTS

Certificate of Examination

This is to certify that the dissertation titled "Morphology Engineering and Catalytic Studies of CuO Nanoparticles Derived from Coordination Polymers" submitted by Mr. Harikrishnan R (MS15057) for the partial fulfilment of BS-MS dual degree programme of the Institute, has been examined by the thesis committee duly appointed by the Institute. The committee finds the work done by the candidate satisfactory and recommends that the report be accepted.

Dr. Ramesh Ramachandran
(Member)

Dr. Ananth Venkatesan
(Member)

Prof. Sanjay K. Mandal
(Supervisor)

Dated: June 15, 2020

Declaration

The work presented in this dissertation has been carried out by me under the guidance of Prof. Sanjay. K. Mandal at the Indian Institute of Science Education and Research Mohali. This work has not been submitted in part or in full for a degree, a diploma, or a fellowship to any other university or Institute. Whenever contributions of others are involved, every effort is made to indicate this clearly, with due acknowledgement of collaborative research and discussions. This thesis is a bonafide record of original work done by me and all sources listed within have been detailed in the bibliography.

Harikrishnan R

Dated: June 15, 2020

In my capacity as the supervisor of the candidate's project work, I certify that the above statements by the candidate are true to the best of my knowledge.

Prof. Sanjay. K. Mandal

Dated: June 15, 2020

Acknowledgements

I would like to express my sincere gratitude to several people who have contributed towards shaping this thesis. The completion of this thesis would have never been possible without their support.

First and foremost, I owe a deep sense of gratitude to my supervisor Prof. Sanjay Mandal for his valuable advice, guidance and consistent encouragement for the past one year. His scholarly inputs and comments helped me building concepts to give an overall direction to this research. I thank him for growing me as a research scientist. This accomplishment has been made possible because of his unconditional support and guidance throughout this time.

I am also grateful to my committee members: Dr. Ramesh Ramachandran and Dr. Ananth Venkatesan. Their brilliant comments and suggestions have encouraged me to carry forward this research with in-depth investigation and analysis.

I also wish to thank former and current Directors of IISER Mohali, for providing the infrastructure and central research facilities at IISER Mohali. I want to acknowledge the former and current Head of the Department, Chemical Sciences, IISER Mohali, for the various departmental facilities.

I express my humble gratitude to Mr. Bahadur, Mr. Mangat, Mr. Satwinder, Mr. Prahlad, Mr. Vishal and Mr. Ganesh (lab assistants of chemistry teaching lab) for their time to time help.

I would like to sincerely acknowledge my current and former lab members, Dr. Sadhika Khullar, Dr. Navnita Kumar, Dr. Sandeep Kashyap, Dr. Biswajit Laha, Dr. Vijay Gupta, Dr. Datta Markad, Dr. Gouri Chakraborty, Dr. Prasenjit Das, Shradha Gandhi, Alisha Gogia, Sheeba Khan, Alokananda Chanda, Himanshi and Vaibhav Pal for their cooperation in creating a good working atmosphere in the lab. I would like to specially thank Alisha Gogia and Sheeba Khan for their love, help, guidance, and support all the time.

Words are inadequate to express my hearty thank to my friend Manu for his presence and support throughout this time. I also want to thank my friends – Nikhil and Aditya for being there always whenever I needed them.

I would also like to say a heartful thanks to my parents for always encouraging me to follow my dreams. I am especially grateful to my father, Raghavan, who has always allowed me to stay as I am and for fulfilling all my dreams whenever I had one. Magical words and love of my mother, Komalavally, has always helped to face every situation I had in my life. Words are inadequate to thank both of them.

Above all, I owe it all to Almighty for granting me wisdom, strength and mercifulness in accomplishing this work.

List of Figures

Chapter I (Introduction)

Chapter III (Results and Discussion)

List of Schemes

List of Tables

Chapter III (Results and Discussion)

Contents

Abstract

The new scientific technologies are the result of human dreams and imagination. The emergence of nanotechnology, a 21st-century frontier, is the outcome of such dreams. Nanotechnology and nanomaterials have become an integral part of human life by providing society with greater benefits. Henceforth, researches on synthesizing and processing diverse range of nanomaterials with unique physical and chemical properties has got significant attention. Metal-Organic Frameworks (MOFs) or Coordination Polymers (CPs) are an important class of compounds because of their various potential applications such as gas storage, separation, catalysis, and sensing. Such porous materials have attracted enormous attention because of their high surface areas, controllable structures, and tunable pore sizes. MOF-based metal oxide nanoparticle synthesis has gained enormous importance due to its less dependence on surfactants or modulators. The hierarchical transfer of morphology and other characteristics from framework to the porous metal oxides makes this approach a unique and more efficient than other existing methodologies.

With these aspects in mind and the quest for some beautiful and fascinating nanomaterials, in this work a strategy of using CPs as the precursors for the formation of metal oxide nanoparticles is developed. In particular, the synthesis of copper oxide (CuO) nanoparticles from CPs using direct calcination method under ambient conditions. These precursor CPs were synthesized at room temperature using metal salts and ligand in a one-pot self-assembly process and characterized using SCXRD, PXRD, TGA, UV-vis and FTIR spectroscopy. These CPs were calcined at various optimized reaction conditions to form CuO nanoparticles and characterized using PXRD, FTIR, SEM, TEM and HRTEM. The effect of temperature and time on the morphology of CuO has been demonstrated.

Due to the Lewis acidic nature of porous CuO nanoparticles, these have been used as heterogeneous catalysts for C-N bond-forming Strecker reaction for the formation of α-aminonitriles under solvent-free conditions. We have found that these porous CuO nanoparticles act as an efficient catalyst with less loading and less reaction time. A broad substrate scope has also been demonstrated showing the versatile nature of CuO nanoparticles as heterogeneous catalysts. Also, the recyclability and stability after more than three cycles further make it a promising candidate in the field for heterogeneous catalysis.

CHAPTER I

INTRODUCTION

"The history of science, like the history of all human ideas, is a history of irresponsible dreams, of obstinacy and of error"- Karl Popper. Nanotechnology emerged in the 21st century is a result of such a dream. The current past in the technological advancement proved that evolution in nanotechnology and nanoscience is the crucial factor. Nanotechnology can be stated as the development, synthesize, characterization and application of materials and devices by modifying their size and shape in nanoscale.[1] The word 'nano' is derived from the Greek word 'nanos', which means 'dwarf', but in science, it means one billionth (10^{-9}). Richard Zsigmondy, the Nobel Prize Laureate (1925) in chemistry, proposed the term 'nanometer'. He was the first person to characterize the size of particles (gold colloids) using a microscope.[2]

The basic and critical elements of nanotechnology are the nanomaterials. Materials whose at least one of the dimension is in the nanoscale regime, 1-100 nm, are usually termed as nanomaterials. Nanotechnology aims at building nanomaterials which are of great scientific interest owing to their unique physical and chemical properties. It plays a crucial role by acting as a bridge between bulk materials and atomic or molecular structures. When a particle goes to its nanoscale range, the principles of classical mechanics can no longer describe its behaviour (movement, energy, etc.) and hence the principles of quantum mechanics get applied. Thus, the materials on the nanometer scale may exhibit physical properties entirely different from those of the bulk.[3] However, the properties of nanomaterials are determined not only by the particle size but also by several other factors: structure, shape and surface status of the particles.[4–6] These nanomaterials include nano-objects such as nanoparticles, nanofibers (rods, tubes) and nanoplates, which consist of different materials, and therefore, derived agglomerates and aggregates.[7–9]

The applications of nanotechnology are spreading in nearly all the branches of science and technology. The difference between the nanoscience and nanotechnology is that the nanoscience gives the knowledge about the arrangement of atoms and their basic properties at nanoscale whereas the nanotechnology is the technology used in governing the matter at the atomic level for the synthesis of the novel nanomaterials with different characteristics.[10]

Numerous synthetic methods are either being developed or improved for the production of nanomaterials. In addition to this, large-scale development in the instrumentation has led to an enhanced nanomaterial characterization and subsequently, their utilization in advance applications. These synthetic methods are further modified to achieve functionalized nanoparticles which have enhanced mechanical, physical, chemical and optical properties.[11] Nowadays, nanoparticles are involved in every part of life, starting from cooking vessel to electronics to pharmaceutics and aerospace industry.[12] It is expected that nanotechnology will bring the next industrial revolution for exponential growth. The world of nanotechnology has an enormous impact on human life, and henceforth, it is the key to a clean and sustainable future.

1.1. Classification of nanomaterials

1.1.1. Based on the origin of nanomaterials

(i) Natural nanomaterials

Nanomaterials which belong to the natural world and have not been processed or engineered by humans are called natural nanomaterials. Due to the inherent nanostructures, these materials possess remarkable properties. These include:

a) **Natural inorganic nanomaterials.** These materials include a broad spectrum of elements, the most common being: - metal oxides/hydroxides (e.g. manganese oxides and hydroxides, iron oxides/oxyhydroxides), metal alloys, silicates (e.g. allophane, fibrous clay minerals, asbestos), sulphides (FeS_2 and ZnS), sulphates, halides and carbonates. The underlying mechanism for the growth of these materials involves nucleation and growth of various inorganic phases in the atmosphere. The inorganic reactions occurring in the hydrosphere and the lithosphere contributes to the generation of these materials via non-thermal, thermal, photochemical and biological processes (Figure 1.1).

b) **Natural organic nanomaterials.** Along with the inorganic nanomaterials, nature is comprised of a wide variety of organic nanomaterials. From the combustion of fossil fuels, the first carbon nanotube and the first buckyball, fullerene, was produced. The volcanic ashes that are released during eruptions contain naturally occurring buckyballs. The petroleum and the natural gas contain various organic nanostructures which get deposited as nanoscale diamond structures.
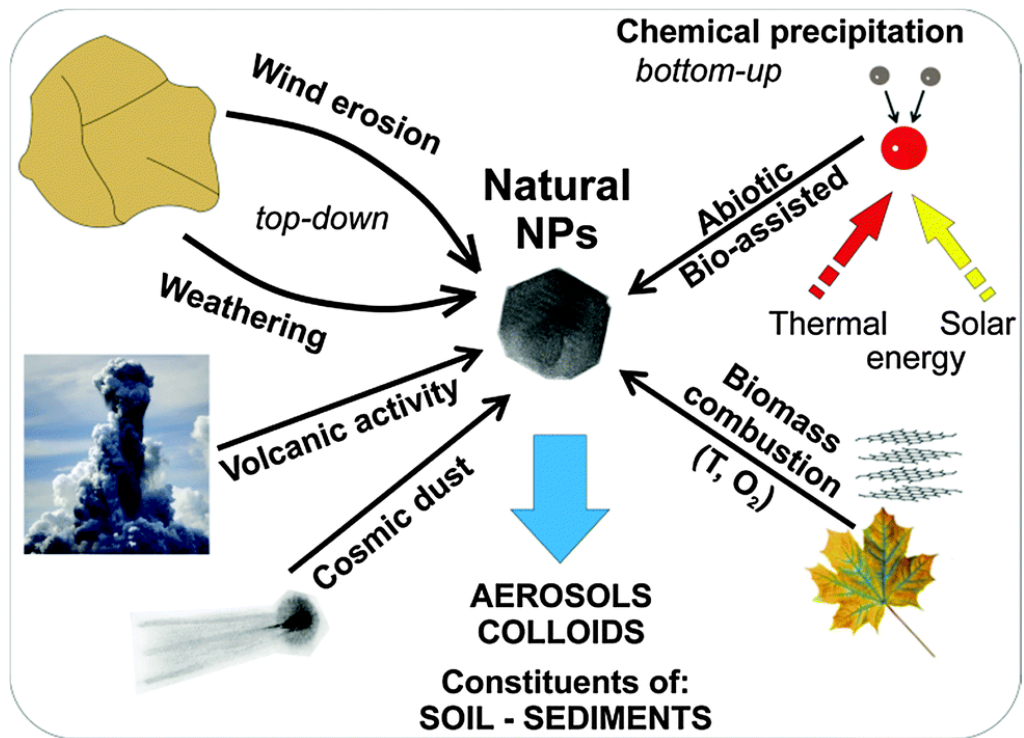
Figure 1.1. Natural processes leading to the formation of inorganic nanomaterials.[13]

(ii) Artificial nanomaterials

These types of nanomaterials are synthesized by different methods. They can be further classified into four classes, as shown in Figure 1.2.
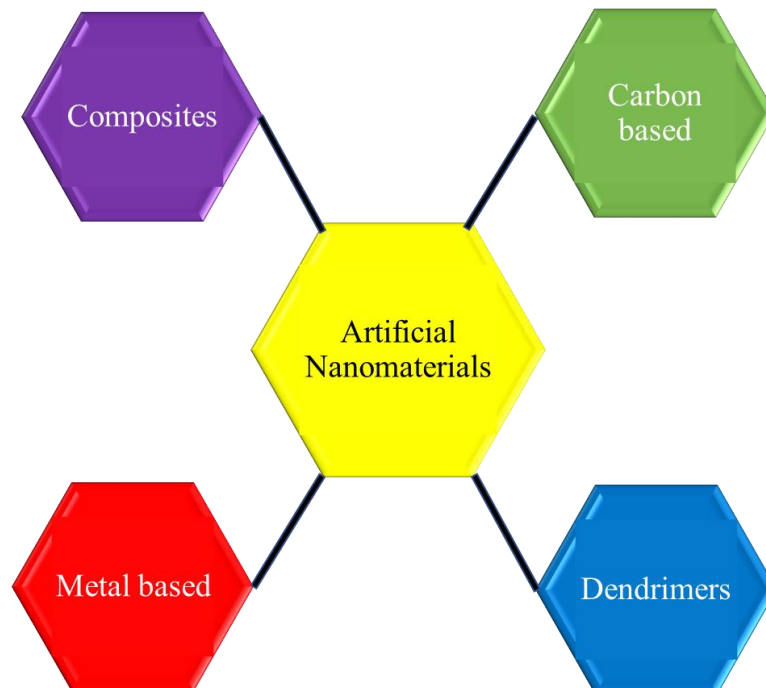

Figure 1.2. Four classes of artificial nanomaterials.

(a) **Carbon-based nanomaterials.** Nanomaterials that are completely composed of carbon are generally classified into this category. They are further classified into carbon nanofibers, carbon nanotubes, fullerenes, graphene and carbon black.[14]

(b) **Composites.** Nanomaterials produced when nanoparticles are incorporated into the matrix of another material are termed as composites. The addition of nanoparticles into another material result in the enhancement of mechanical, physical, chemical, and electrical properties. For example, nanosized clays are incorporated to a wide variety of materials including packaging materials and auto parts to enhance their desired properties.[15]

(c) **Dendrimers.** These are highly branched materials composed of nanosized polymers. A dendrimer structure has three main parts; a central core part, an inner branched part (dendritic structure), and an outer surface consisting of numerous chain end. These chains can be altered to produce process-specific dendrimers which can be used in different areas such as catalysis and sensing. Additionally, the inner part can be utilized in trapping molecules, henceforth, can be used in targeted drug delivery.[16]

(d) **Metal-based nanomaterials.** Nanomaterials that are synthesized from metals are generally classified as metal-based nanomaterials. Most of the metals can be converted into their respective nanoparticles. For example, nano-lead, nano-gold, and metal oxides, such as zinc oxide. Metal oxide based nanomaterials are preferred over metals because of their high reactivity and efficiency.[17,18]

1.1.2. Based on dimensions of nanomaterials

Nanomaterials can also be classified based on the dimension of the particles, as shown in Figure 1.3. Examples of such nanomaterials are shown in Figure 1.4.

(i) **Zero dimensional (0D) nanomaterials.** These are class of materials whose all the dimensions are measured within the nanoscale, 1-100 nm. For example, quantum dots, fullerenes, metal nanoparticles such as nano-platinum, nano-iron, nano-silver, etc.

(ii) **One dimensional (1D) nanomaterials.** These are class of materials whose one of their dimensions is outside the nanoscale (greater than 100 nm) while the other two

dimensions are in the nanoscale, 1-100 nm. For example, nanotubes, nanorods, nanowires, etc.

(iii) Two dimensional (2D) nanomaterials. In this class of materials, two dimensions are out of the nanoscale (greater than 100 nm) and one dimension in the nanoscale (1-100 nm). For example, nanofilms, nanolayers, nanoplates, graphene sheets, etc.

(iv) Three dimensional (3D) nanomaterials. These are class of materials whose all the dimensions are out of the nanoscale (greater than 100 nm). For example, liposomes, dendrimers, nanoflowers, nanocones, etc.
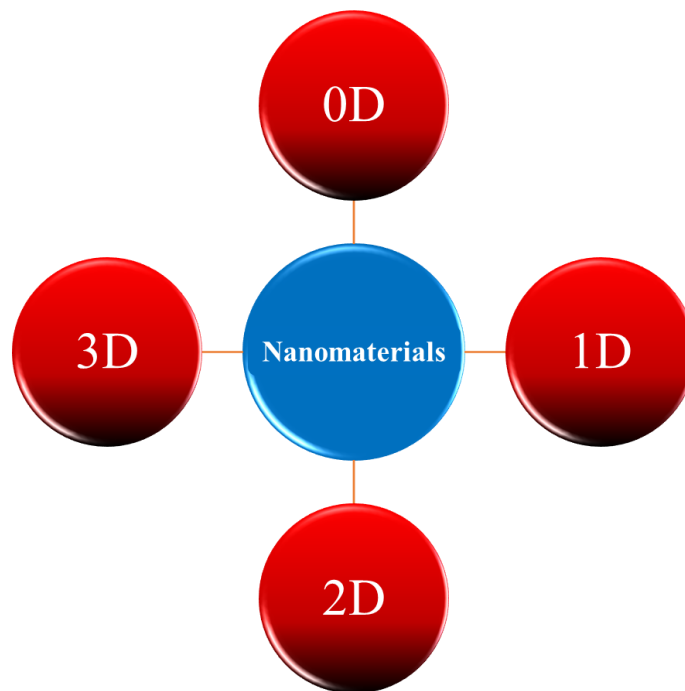
Figure 1.3. Classification of nanomaterials based on dimension.

1.2. General methods for the synthesis of nanomaterials

In general, there are two approaches for the synthesis and fabrication of nanomaterials which are as follows (Figure 1.5):

(i) Bottom-up approach. The bottom-up or constructive method is the build-up of material from atom to clusters to nanoparticles. This approach has been proved to be more favourable for the synthesis of nanoparticles. Different techniques have been developed to synthesize the nanomaterials using this approach. Typical examples are the formation of nanoparticles from colloidal dispersions.

(ii) Top-down approach. The top-down or destructive method is the reduction of bulk material to nanometric scale particles.

5
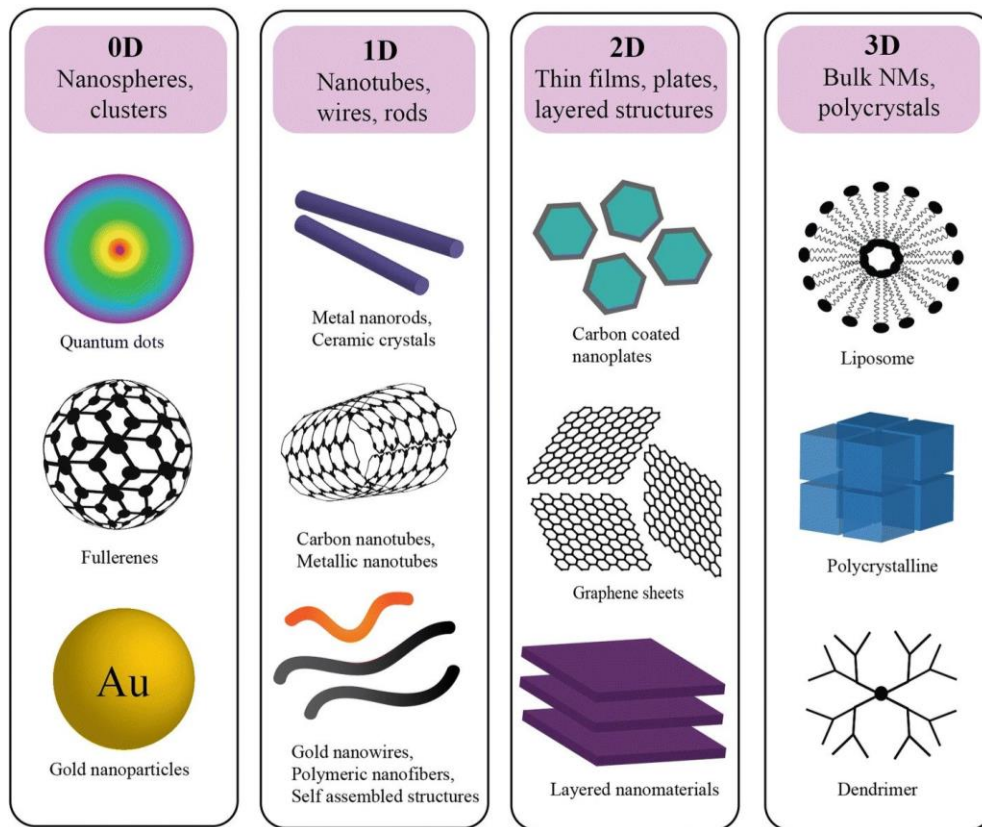
Figure 1.4. Examples of 0D, 1D, 2D, and 3D nanomaterials.[19]
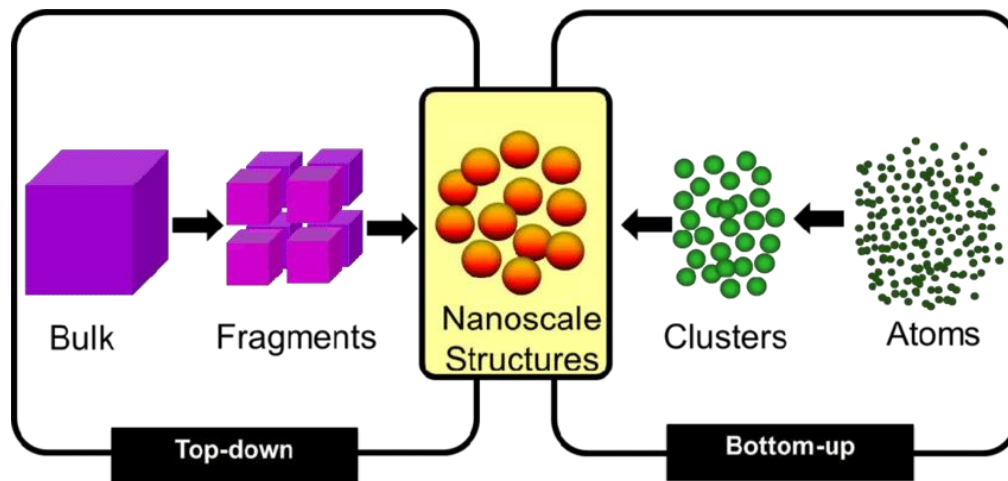
Figure 1.5. Bottom-up and top-down approaches for the synthesis of nanmaterials.[20]

1.3. Synthetic techniques of nanomaterials

There are different synthetic techniques that can be used for the synthesis of nanomaterials (Figure 1.6). It includes mechanical methods and lithographic techniques under the top-down approach and vapour phase, chemical phase and self-assembly techniques under the bottom-up approaches as listed below:
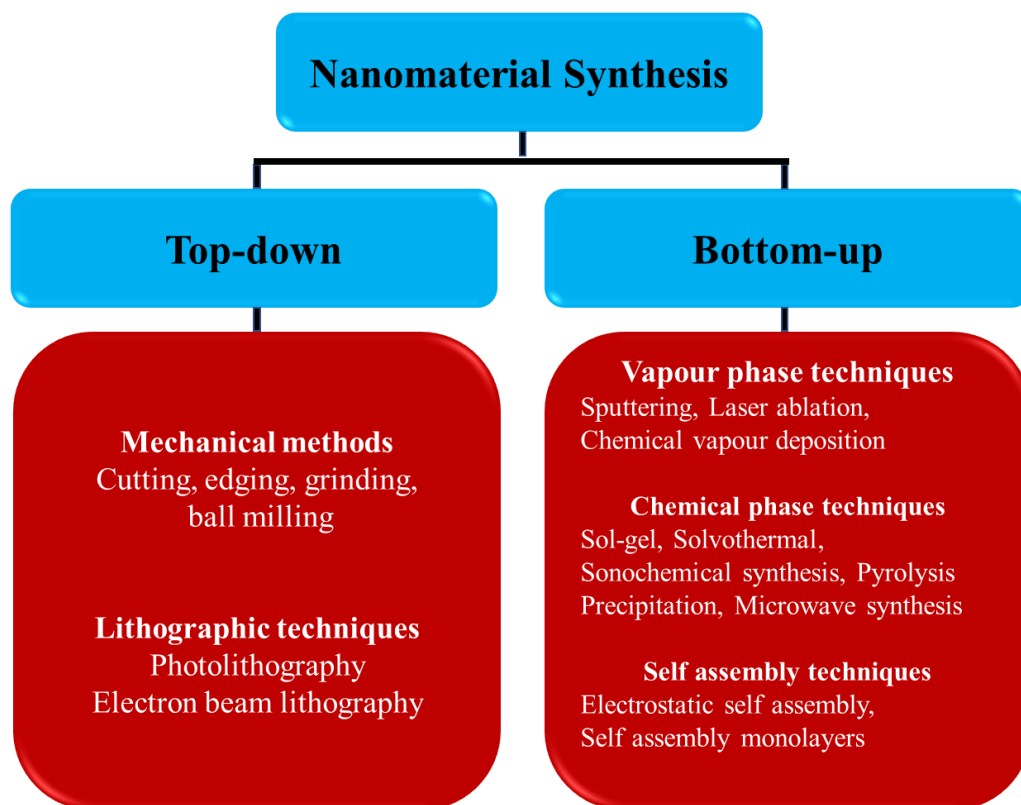
Figure 1.6. Different methods for the nanomaterial synthesis.

(i) Ball milling

In this process, the bulk material (i.e. powder mixture) is placed in the ball mill containing balls which rotate with high energy and crushes the solid material into nanocrystallites. [21]

(ii) Electron beam lithography

A highly focused beam of electrons is used to write out a pattern on a surface covered with an electron sensitive film called a resist. This electron beam can induce a change in the molecular structure and solubility of the resist film. The resist film can further be immersed in a solvent for the selective removal of either the exposed or the non-exposed regions.[22]

(iii) Hydrothermal/Solvothermal method

This is a solution-based approach for synthesizing nanomaterials using pressurized vessels called autoclaves that can withstand high temperature and pressure for a long time (Figure 1.7). Materials which are practically insoluble under normal conditions such as oxides, sulphides, silicates, etc. can be synthesized using this technique.[23]

Figure 1.7. a) Steel jacket and b) Teflon reactor used for the Hydrothermal method.

(i) Pyrolysis

Pyrolysis is one of the most widely used synthetic method the largescale production of nanoparticles in industries. In a typical synthesis, a precursor, which can be solid, liquid, or vapour is burned using a flame. The precursor is inserted into a furnace, which can go to very high temperatures, through a small hole and is allowed to burn.[24] The combustion of by-product gases is then air classified to recover the nanoparticles. Furnaces that use plasma and laser instead of flame are prevalent due to their capacity to produce high temperature, which can enhance the evaporation. Pyrolysis, as a synthetic method, has got wide acceptance owing to their advantages as a simple, efficient, cost-effective method which involves a continuous process to give with high yields of product.[25] A photograph of the tube furnace used in this is work is shown in Figure 1.8.

Figure 1.8. Photograph of tube furnace used for pyrolysis.

(ii) Laser ablation

Laser Ablation Synthesis in Solution (LASiS) is a unique method used for the synthesis of nanoparticle from various solvents. Here, the desired metal immersed in an appropriate liquid solution is irradiated by a laser beam which upon condenses a plasma plume that can produce nanoparticles.[26]

1.4. Metal Oxide Based Nanomaterials

In the recent past, metal oxide nanostructures have received significant interest from the research community on account of their exceptional physical and chemical characteristics emerging from the quantum realms in the nano dimension.[27] Metal oxides are different from their corresponding metals in various aspects such as their intrinsic charge separation capacity, and this difference increases in the nanoscale. Metal oxide nanoparticles have already received much appeal due to their wide application in the areas of electronics[28], optics[29], energy storage industry[30] and catalysis[31]. However, the synthetic approaches for metal oxide nanoparticles for desired properties are still to be explored.

The research on metal oxide nanoparticles includes their synthesis from different methodologies, along with their physical, chemical, and structural characterization. In addition, their application in various fields of technology and inherent self-assembly properties to produce multi-dimensional superstructures are also investigated. The current research in nanomaterials are concentrated in developing new synthetic routes, which is also necessary, however, detailed understanding of the underlying physical, chemical, and structural properties is crucial in developing as-synthesized nanomaterials into various technological applications.

Among the metal oxide materials, copper (II) oxide (CuO), a semiconductor with a narrow bandgap energy of ~1.2 eV has achieved enormous importance due to their discrete properties and applications in various fields.[32,33] Excellent stability in solutions, specific redox potential, high surface area, and excellent electrochemical properties are some of these properties.[34,35] Although different synthetic strategies, hydrothermal[36], sonochemical[37], electrostatic coprecipitation[38], etc. has been reported for CuO nanostructures; it is still difficult to have control over the size and shape of the as-synthesized CuO nanostructures simultaneously.[39] Fabricating nanoparticles with desirable properties needs precise control over the synthetic strategies, which in turn result in the formation of different copper oxide nanostructures with controllable dimensions. Over the

past decade Copper oxide nanostructures with different morphology such as nanowires[40], nanocubes[41], nanoribbons[42],nanoflowers[43], nano-octahedra[44], nanoshuriken[35], and nanofilms[45] have been synthesized, each through different methods such as colloidal synthesis, solvothermal, thermal oxidation, template synthesis, and sonochemical techniques[40]. From sensing to therapeutics, CuO nanoparticles have proven its vital importance in developing new technologies in various fields and upgrading the existing ones.

1.5. Motivation

The present work is based on the synthesis of nano metal oxides using metal-organic coordination networks as the precursors through the bottom-up approach, the most favourable approach for the synthesis of nanomaterials. Metal-organic coordination networks (MOCNs) have been widely researched owing to their specific structures, tailorable properties and potential applications in separation, storage devices, catalysis, sensors and synthesis of nanomaterials. These MOCNs can act as sacrificial templates to obtain the nanomaterials with desired morphologies. The usual approach for the preparation of nano metal oxides consists of the thermal decomposition of these MOCNs at higher temperatures. At such high temperatures, the metal species acquire sufficient mobility, whereas the organic linker in MOCNs gets burnt away, leading to the rupture of the framework.[46] Once the framework is decomposed, carbon and nitrogen present in these MOCNs get oxidized into their respective oxidized gases. The carbon formed during the thermolysis also acts as a reducing agent for the reduction of metal oxides by a simple carbothermic reaction. Thus, MOCNs may be envisioned as suitable precursors for the formation of highly stable nanomaterials bearing catalytic properties. Moreover, the synthetic method followed, direct calcination, has the advantages of being a simple, cost-effective, efficient, and continuous method to give with high yields of product.[47] Amino acids have got wide importance due to their particular ability to act as a hydrogen bond donor and acceptor along with exhibiting different binding modes with the metal center by utilizing the several functionalities present in the system. Moreover, amino acids are readily available at low cost, making them a suitable precursor for the synthesis of the ligand.

1.6. Present work

In this work, the synthesis of copper oxide nanostructures by the calcination of two different amino-acid ligand-based coordination polymers is reported. The heating rate, annealing

temperature and time of calcination have a crucial role in the synthesis and morphology of the final product. The high crystallinity of these nanoparticles was confirmed by the Powder X-ray diffraction (PXRD) studies. These were further characterized using FT-IR spectroscopy, Field Emission Scanning Electron Microscopy (FESEM) and Transmission Electron Microscopy (TEM) analysis. The morphological transformation of one of the as-synthesized copper oxide nanostructures is studied. In addition, these nanoparticles were used as a heterogeneous catalyst in C-N bond-forming Strecker reaction. Our results showed that copper oxide nanoparticle is an excellent catalyst for this reaction.

CHAPTER II

EXPERIMENTAL SECTION

2.1 Materials and methods

All the chemicals and solvents used for this work are of analytical grade, were obtained from commercial sources, and were used as received, without further purification. All rection except Strecker reaction was carried out in the aerobic condition. Strecker reaction was carried out in a Schlenk tube under nitrogen atmosphere.

2.2 Physical measurements

NMR spectra of the synthesized ligands were obtained in deuterated solvents at 25 °C on a Bruker ARX-400 spectrometer; chemical shifts are reported relative to the residual solvent signals. Each sample was prepared by taking 5-10 mg of the compound in approx. 0.5 mL of the deuterated solvent. Each data obtained was analyzed and plotted using either MestReNova or Spinworks.

Melting points (M.p.) were measured on a Büchi Melting and Boiling Point apparatus. All melting points have been measured in open melting point capillaries.

FT-IR spectra were measured in the range of 4000-400 cm^{-1} on a Perkin-Elmer Spectrum I spectrometer with samples prepared as KBr pellets.

Thermogravimetric analysis was carried out from 25 to 500 °C (at a heating rate of 10 °C/min) under dinitrogen atmosphere on a Shimadzu DTG-60. The sample to be analyzed was weighed using an analytical balance, put in a pan and weighed again using the microbalance of the instrument to avoid any discrepancy. The data obtained were analyzed using the TA 60 software.

Powder X-ray diffraction data were recorded on a Rigaku Ultima IV diffractometer equipped with a 3 kW sealed tube Cu Kα X-ray radiation (generator power settings: 40 kV and 40 mA) and a DTex Ultra detector using parallel beam geometry (2.5° primary and

secondary solar slits, 0.5° divergence slit with 10 mm height limit slit). For room temperature measurements, samples were grounded into a fine powder using a mortar and a pestle and was placed on a glass sample holder. The data were collected over an angle range 20° to 80° with a scanning speed of 2° per minute with 0.02° step.

Field Emission Scanning Electron Microscopy (FESEM) was performed on a JEOL instrument; samples were well dispersed in MeOH and drop cast on a silicon wafer, dried and sputtered with gold for a time period of 20 seconds for increasing the conductivity of the sample and a working distance of 4.5 to 15 mm was used with a voltage of 10 to 15 kV and probe current of 6 amp.

Energy dispersive X-ray (EDX) spectroscopy was carried out on a HORIBA EX-250 instrument (15 kV) associated with FESEM

Transmission electron microscopy (TEM) was performed on FEI Tecnai G2 F20 equipped with a field emission gun operated at 200 kV with 1 mg sample well dispersed in MeOH (10 mL) using a sonicator for 30 minutes. The sample was then drop casted on a copper grid, followed by drying using a lamp for 30 minutes.

2.3 Synthesis of precursors

The amino-acid based ligands and their coordination polymers are synthesized following the reported procedure.[48]

2-(benzylamino)-3-(4-hydroxyphenyl)propanoic acid (L-H$_2$Tyrbenz): In a 25 mL round bottom flask, benzaldehyde (0.28 mL, 2.8 mmol) was added to a solution of L-tyrosine (507 mg, 2.8 mmol) and NaOH (224 mg, 5.6 mmol) in 14 mL of the methanol-water mixture (v/v 1 : 1). The resulting solution was refluxed for 1 h. The yellow reaction mixture was brought to room temperature prior to the addition of NaBH$_4$ (105 mg, 4.8 mmol) at 0 °C. The solution was stirred until the yellow colour disappeared. The pH was adjusted to 5 using (~2 mL) glacial acetic acid, and the solution was stirred for half an hour. The white precipitate was filtered off, washed with water and air-dried. Yield: 70 % (535 mg), Melting point: 260 °C.

3-(4-hydroxyphenyl)-2-((thiophen-2-ylmethyl)amino)propanoic acid (L-H$_2$Tyrthio): In a 25 mL round bottom flask, 2-thiophenecarboxaldehyde (0.30 mL, 2.8 mmol) of was added to a solution of L-tyrosine (507 mg, 2.8 mmol) and NaOH (224 mg, 5.6 mmol) in 14 mL of the methanol-water mixture (v/v 1 : 1). The resulting solution was refluxed for 3

h. The yellow reaction mixture was brought to room temperature prior to the addition of NaBH$_4$ (105 mg, 4.8 mmol) at 0 °C. The solution was stirred until the yellow colour disappeared. The pH was adjusted to 5 using (~2 mL) glacial acetic acid, and the solution was stirred for half an hour. The white precipitate was filtered off, washed with water and air-dried. Yield: 70 % (529 mg), Melting point: 248 °C.

{[Cu(L-HTyrbenz)$_2$]·CH$_3$OH·H$_2$O}$_n$ (CP-1): In a 10 mL round bottom flask, L-H$_2$Tyrbenz (25 mg, 0.092 mmol) and KOH (5 mg, 0.092 mmol) were dissolved in 3 mL methanol. To this, CuSO$_4$·5H$_2$O (16.2 mg, 0.046 mmol) was added with stirring. The reaction mixture turned blue and was stirred for 6 h. After filtering off the K$_2$SO$_4$ precipitate, the blue filtrate was evaporated to dryness to obtain the product. Yield**:** 55 % (16.5 mg).

{[Cu(L-HTyrthio)$_2$]·H$_2$O}$_n$ (CP-2): In a 10 mL round bottom flask, L-H$_2$Tyrthio (25 mg, 0.092 mmol) and KOH (5 mg, 0.092 mmol) were dissolved in 3 mL water. To this, CuSO$_4$·5H$_2$O (11.2 mg, 0.045 mmol) was added of with stirring. The reaction mixture turned green and was stirred for 3 h. After filtering off the K$_2$SO$_4$ precipitate, the green filtrate was evaporated to dryness to obtain the product. Yield**:** 84 % (24 mg).

2.4 Synthesis of CuO nanoparticles

General method: In a typical synthesis, the metal complex was placed in a ceramic boat and then transferred into a horizontal tube furnace and calcined at 550 °C for 4 h at a heating rate of 60 °C/h. The black products obtained was washed with distilled water and absolute methanol several times, after that dried at 60 °C for 6 h to obtain the CuO nanoparticles.

CuO-1: It was followed by the general method using {[Cu(L-HTyrbenz)$_2$]·CH$_3$OH·H$_2$O}$_n$ (40 mg, 0.061 mmol) as metal complex and followed the Program A for heating and cooling in a tube furnace. Yield; 7 mg (75 %)

Program A

1) 30 °C - 550 °C, rate = 60 °C/ h

2) 550 °C for 4 h

3) 550 °C - 30 °C, rate = 60 °C/ h

CuO-2: It was followed by the general method using $\{[Cu(L\text{-}HTyrthio)_2]\cdot H_2O\}_n$ (40 mg, 0.064 mmol) as metal complex and followed the Program B for heating and cooling in a tube furnace. Yield; 7 mg (75%)

Program B

1) 30 °C - 800 °C, rate = 60 °C/ h

2) 800 °C for 5.5 h

3) 800 °C - 30 °C, rate = 60 °C/ h

2.5 Typical experimental procedure for the Strecker reaction

In a typical reaction, a mixture of aldehyde/ ketone (0.1 mmol), aniline (0.1 mmol), TMSCN (0.12 mmol), and CuO nanoparticles (5 mg, 6 mol%) of was stirred at room temperature (25 °C -30 °C) for 1 h under nitrogen atmosphere in a solvent-free condition. Thereafter, 1 ml dichloromethane (DCM) was added to the reaction mixture, and the solid catalyst was separated from the mixture by centrifugation. The supernatant obtained was dried, and the crude product was dissolved in $CDCl_3$ for analyzing. The solid catalyst thus obtained was washed with chloroform, centrifuged and dried and was used again.

CHAPTER III

RESULTS AND DISCUSSION

1. Synthesis and Characterization

Coordination polymers were prepared from their respective amino-acid based ligands through a one-pot two-component reaction at room temperature with high yield. Amino acids have got wide importance due to their particular ability to act as a hydrogen bond donor and acceptor along with exhibiting different binding modes with the metal center by utilizing the several functionalities present in the system. Moreover, amino acids are readily available at low cost, making them a suitable precursor for the synthesis of the ligand. The synthetic procedures followed for the preparation of coordination polymers can be efficiently scaled-up in high yields at room temperature. Henceforth, these reactions can be recognized as green synthesis due to the utilization of safer solvents and chemicals, less hazardous chemical synthesis, and the involvement of an energy efficient process. Further, the as-prepared coordination polymers were used as precursors for the synthesis of metal oxide nanoparticles through direct calcination method, which is a simple, cost-effective, efficient and continuous method to give with high yields of product (Scheme 3.1).

Scheme 3.1. Synthesis of nanoparticles from their precursor coordination polymer
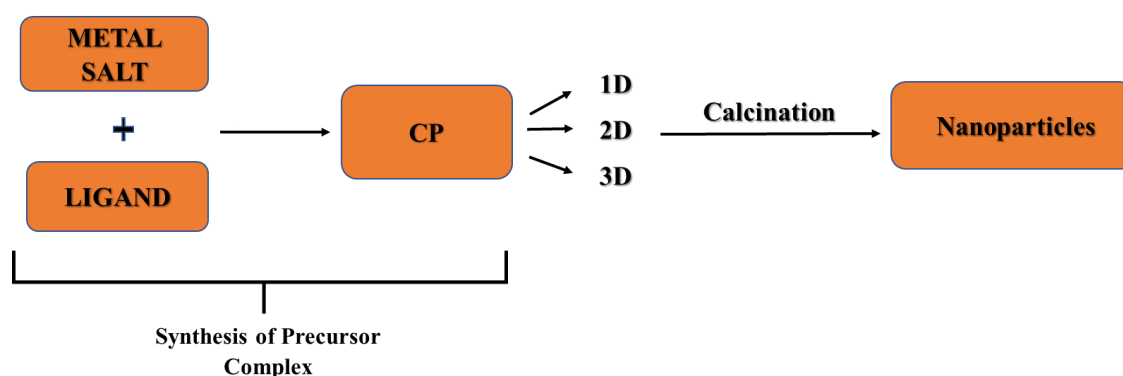
1.1. Precursors

1.1.1. Ligands

1.1.1.1. *Synthesis*. Ligands were prepared from their corresponding amino acid, as shown in Scheme 3.2 and Scheme 3.3. The sodium salt of the L-amino acid was refluxed with the suitable aldehyde in aqueous methanol to obtain the respective Schiff base. The as-obtained Schiff base was further reduced using sodium borohydride, followed by the acidification using glacial acetic acid yielded the desired product. Both the products were obtained as white precipitates, which upon washing with water and air-dried yielded the isolated pure products with excellent yields.

Scheme 3.2. Synthesis of L-H$_2$Tyrbenz
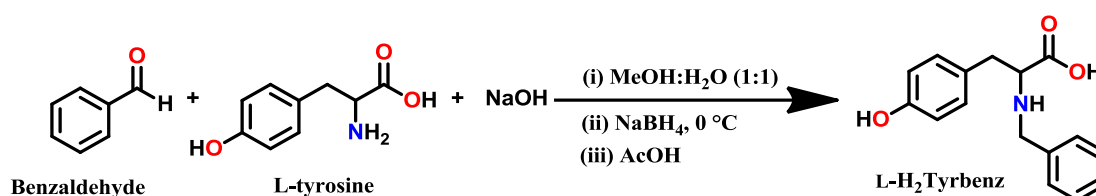
Scheme 3.3. Synthesis of L-H$_2$Tyrthio
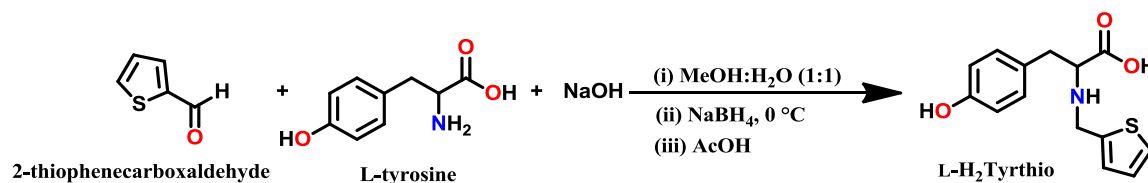
1.1.1.2. *Characterization of ligands*. The synthesized ligands were characterized using FT-IR and NMR spectroscopy.

1.1.1.2.1. *FT-IR spectroscopy*. The FT-IR spectra of both ligands (Figure 3.1 and Figure 3.2) were recorded in the solid-state as KBr pellets in the 400-4000 cm^{-1} range. The FT-IR spectra of both ligands have been compared with the FT-IR spectra of the ligands reported in the literature.[48] For L-H$_2$Tyrbenz, the peaks at 1590 cm^{-1} and 1397 cm^{-1} corresponds to the asymmetric and symmetric stretch of the carboxylate respectively. For L-H$_2$Tyrthio, the peaks at 1582 cm^{-1} and 1394 cm^{-1} corresponds to the asymmetric and symmetric stretch of the carboxylate respectively. The peaks at 1106 cm^{-1} and 717 cm^{-1} for L-H$_2$Tyrthio is due to the C=S and C-S stretch of the thiophene ring.
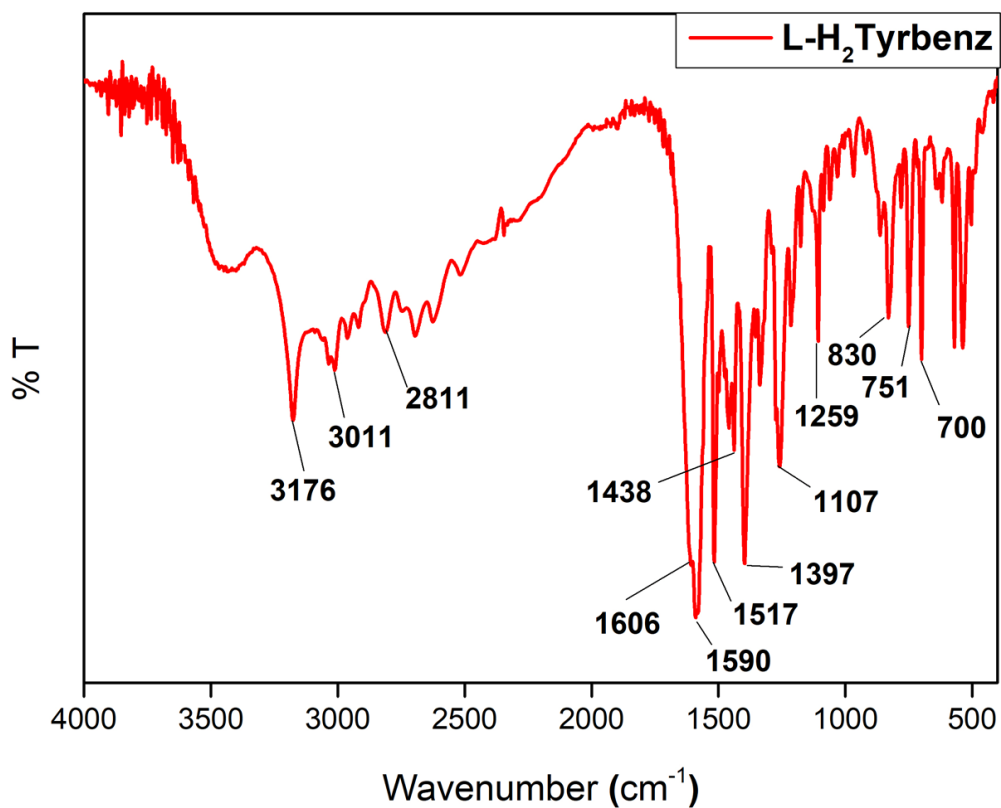
19

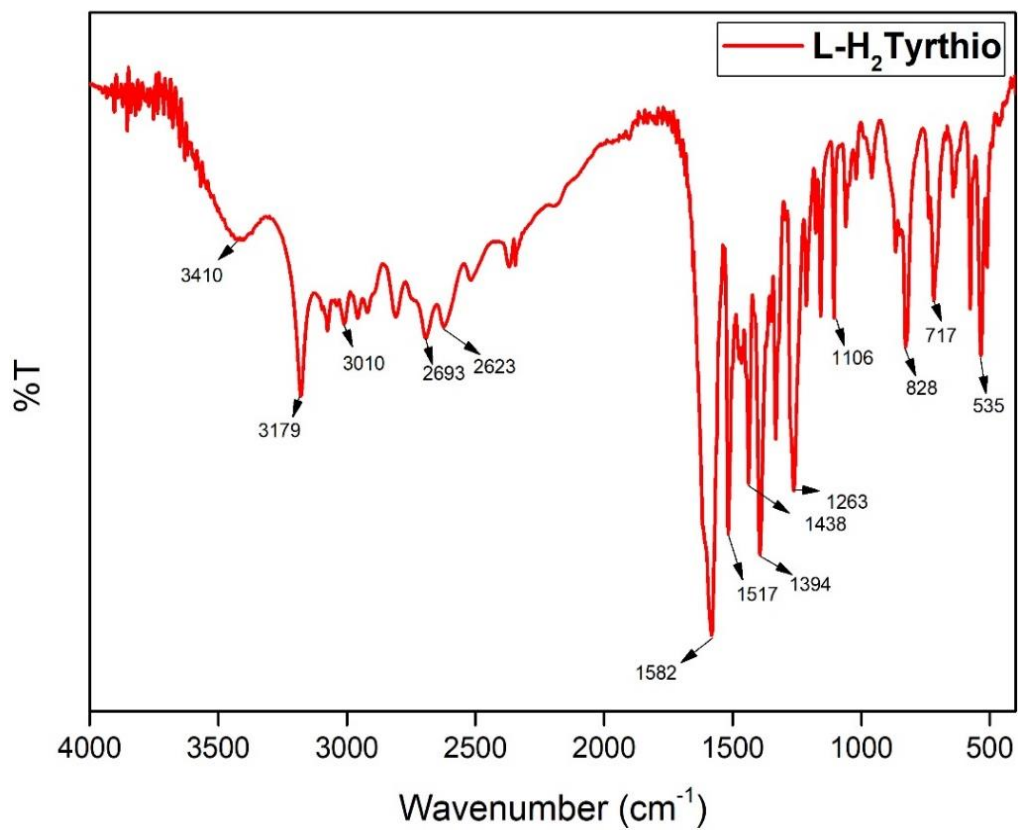.**Figure 3.1.** FT-IR spectrum of L-H$_2$Tyrbenz.

Figure 3.2. FT-IR spectrum of L-H$_2$Tyrthio.

1.1.1.2.2. *NMR spectra.* The ^{1}H NMR spectra of the ligands (Figure 3.3 and Figure 3.4) have been compared with the ^{1}H NMR spectra of the ligands reported in the literature.[48] The formation of both ligands was confirmed using ^{1}H NMR spectra. The spectra were clear, with no extra peaks, showing the high purity of the prepared ligand. The peak at 4.75 ppm in both spectra corresponds to the residual solvent peak (D_2O).
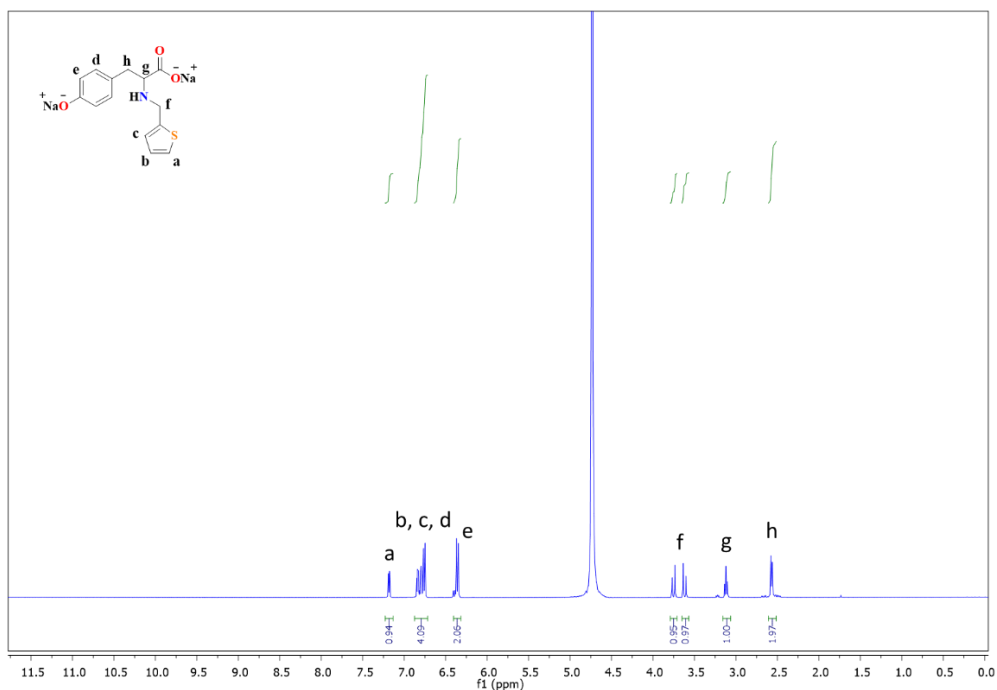

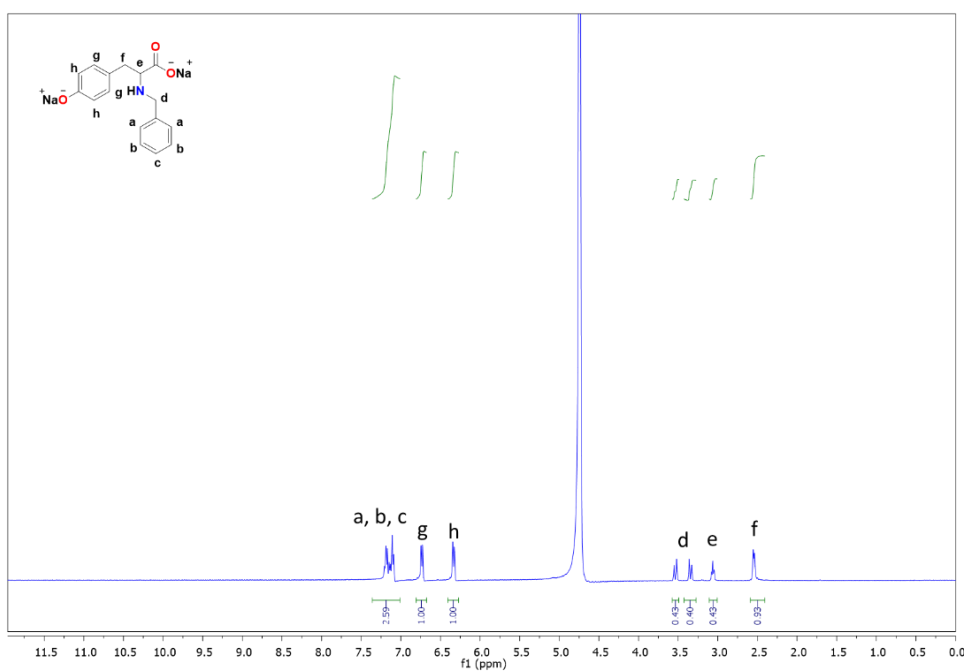**Figure 3.3.** ^{1}H NMR spectrum of L-Na_2Tyrbenz in D_2O.

Figure 3.4. ^{1}H NMR spectrum of L-Na_2Tyrthio in D_2O.

21

1.1.2. Metal complexes

1.1.2.1. *Synthesis.* The metal complexes were synthesized and isolated by a one-pot self-assembly reaction between $CuSO_4 \cdot 5H_2O$ and the respective monopotassium salt of the ligand in a 1:2 ratio in the suitable solvent under ambient conditions (Scheme 3.4). The solvent for the reaction was selected based on the solubility of the final product, the metal complex, and the by-product, K_2SO_4. Unlike **2**, **1** was found to be moderately soluble in water. Thus for **1**, methanol was used as a solvent where the product is soluble, and the K_2SO_4 by-product is insoluble. Here, the precipitate was filtered off, and the blue solution was evaporated under reduced pressure to obtain the desired product. On the other hand, for **2**, water was used as solvent where the by-product K_2SO_4 is soluble, and the product is insoluble, obtained as direct precipitates. The green precipitate was filtered off, washed with water and air-dried to obtain the desired product. Both **1** and **2** were obtained as pure products in good yields, 55 % and 84 %, respectively. Both reactions can be recognized as green synthesis due to the utilization of safer solvents and chemicals, less hazardous chemical synthesis, and the involvement of an energy efficient process.

Scheme 3.4. Synthesis of $\{[Cu(\text{L-HTyrbenz})_2]\cdot CH_3OH \cdot H_2O\}_n$ (**1**) and $\{[Cu(\text{L-HTyrthio})_2]\cdot H_2O\}_n$ (**2**)
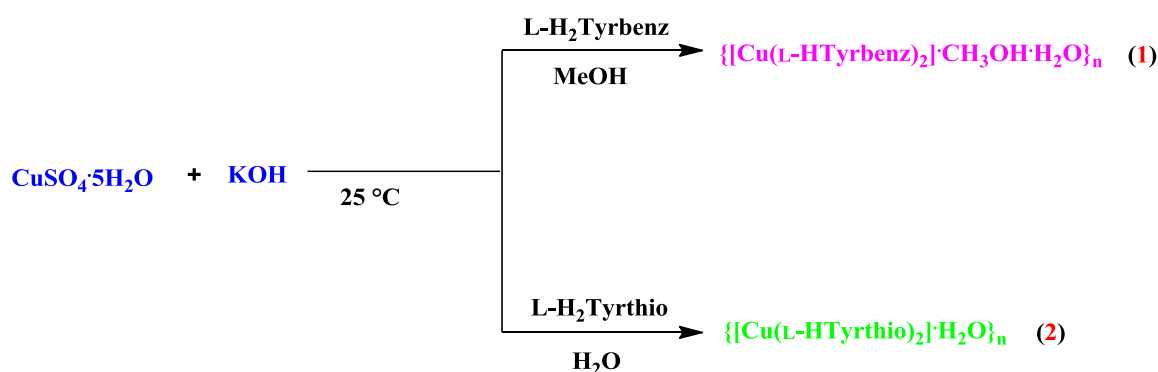
1.1.2.2. *Characterization.* The as-synthesized metal complexes were characterized by FT-IR spectroscopy and Thermo-gravimetric analysis (TGA).

1.1.2.2.1. *FT-IR spectroscopy.* The FT-IR spectra of both CP's (Figure 3.5 and Figure 3.6) were recorded in the solid-state as KBr pellets in the 400-4000 cm^{-1} range. The FT-IR spectra of **1** and **2** have been compared with the FT-IR spectra of the metal complex in the reported literature.[48] For **1,** the peaks at 1628 cm^{-1} and 1376 cm^{-1} corresponds to the asymmetric and symmetric stretch of the carboxylate respectively. Similarly, for **2 t**he

peaks at 1637 cm^{-1} and 1370 cm^{-1} correspond to the asymmetric and symmetric stretch of the carboxylate respectively. The shift in these peaks compared to their respective ligands is due to the binding of the copper metal centre with the carboxylate of the ligand. The difference between asymmetric and symmetric stretching is around 252 cm^{-1} and 267 cm^{-1} for **1** and **2,** respectively, indicates that the binding of carboxylate is in monodentate fashion in both compounds. In the FT-IR spectra of **1** and **2**, the broad peak in the range 3300 cm^{-1} – 3400 cm^{-1} is due to the lattice water molecules. The stretching frequencies for phenolic - OH groups appear at 3262 cm^{-1} (**1**) and 3243 cm^{-1} (**2**). The peaks at 1244 cm^{-1} (**1**) and 1243 cm^{-1} (**2**) is due to the C-O stretching.
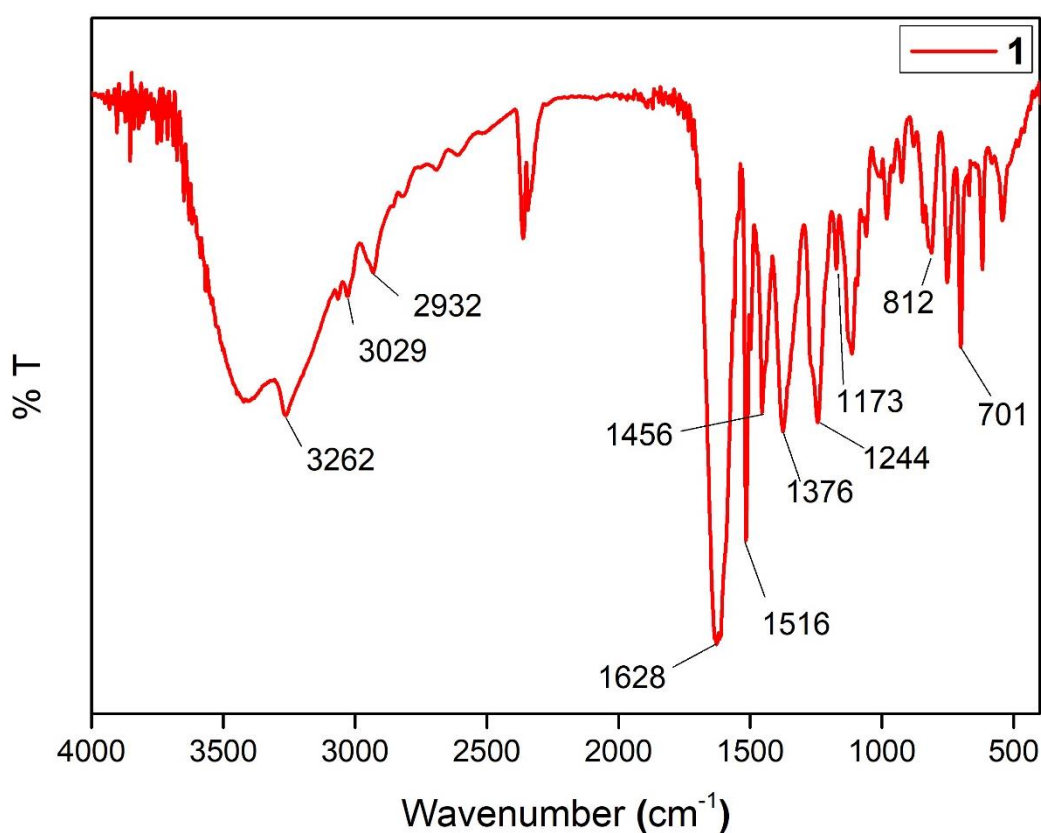

Figure 3.5. FT-IR spectrum of {[Cu(L-HTyrbenz)$_2$]˙CH$_3$OH˙H$_2$O}$_n$.

1.1.2.2.2. *Thermogravimetric analysis.* The thermal stabilities of **1** and **2** (Figure 3.7 and Figure 3.8)   were studied as a function of temperature in the range of 25–500 °C under a nitrogen atmosphere at a rate of 10° per minute. The TGA of **1** and **2** has been compared with the TGA of the metal complex in the reported literature.[48] **1** and **2** show similar thermal stability behaviour with a three-step weight loss profile and thermal stability up to around 200 °C. The weight loss around 100 °C is due to the loss of lattice solvent molecules. The weight losses after 200 °C indicates the further degradation of the compounds.

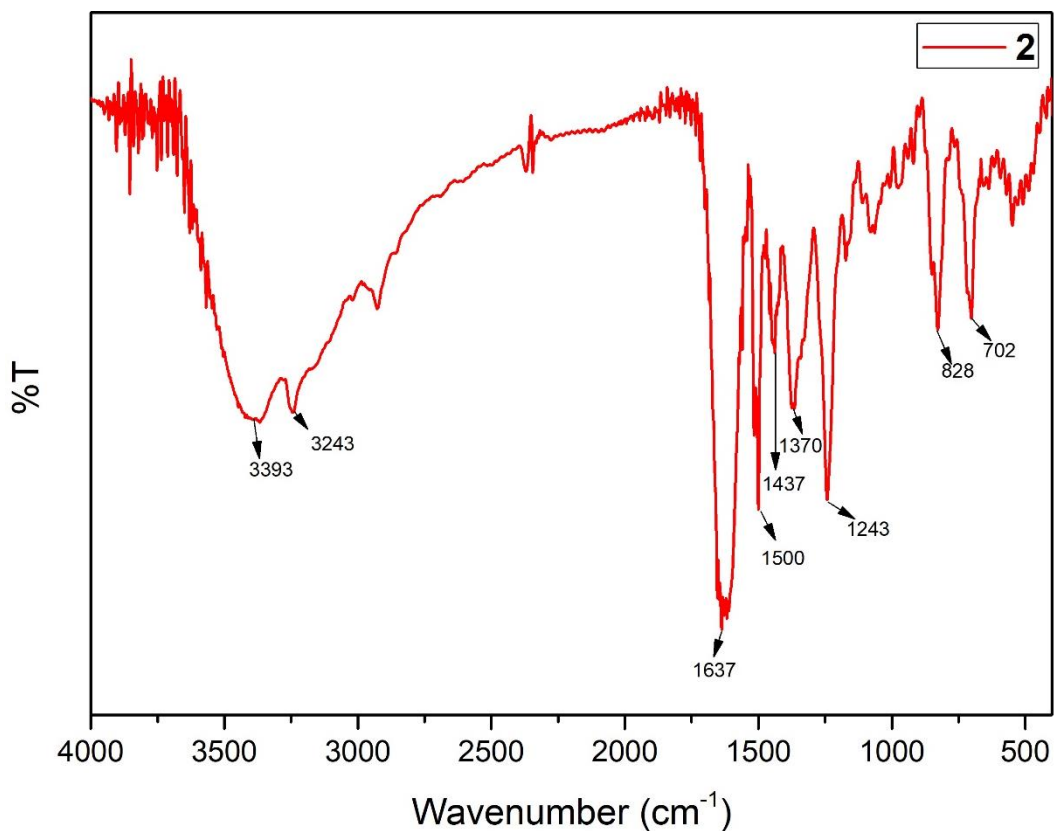**Figure 3.6.** FT-IR spectrum of $\{[Cu(L\text{-}HTyrthio)_2]\cdot H_2O\}_n$.

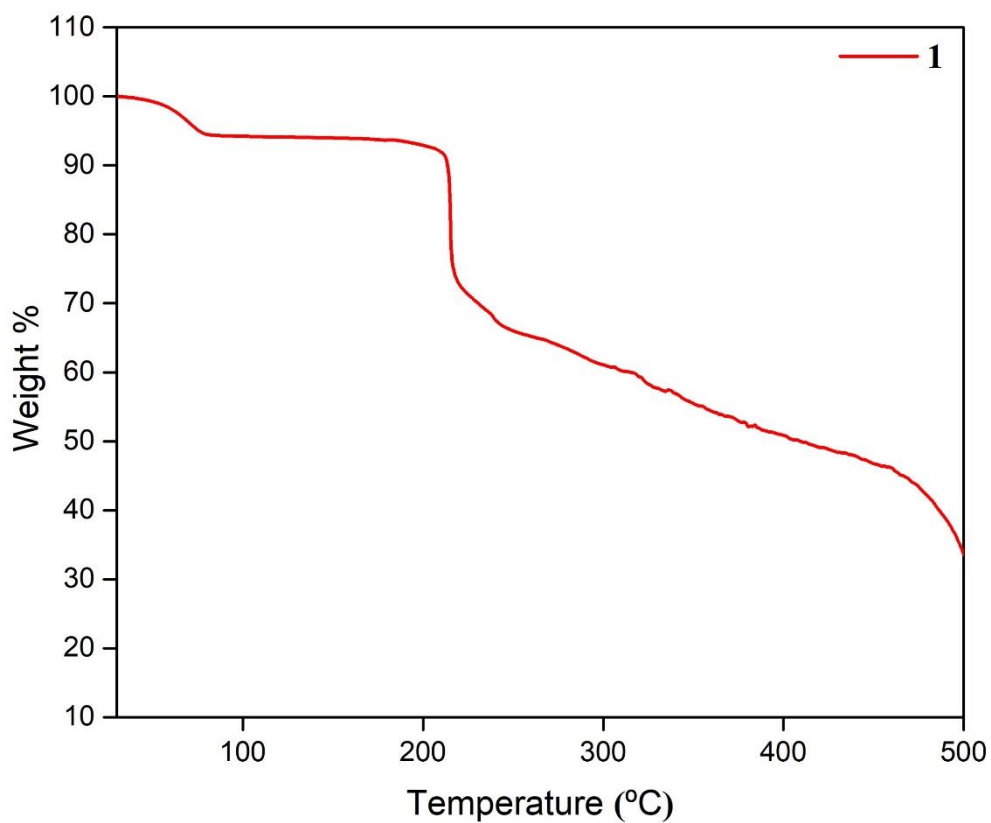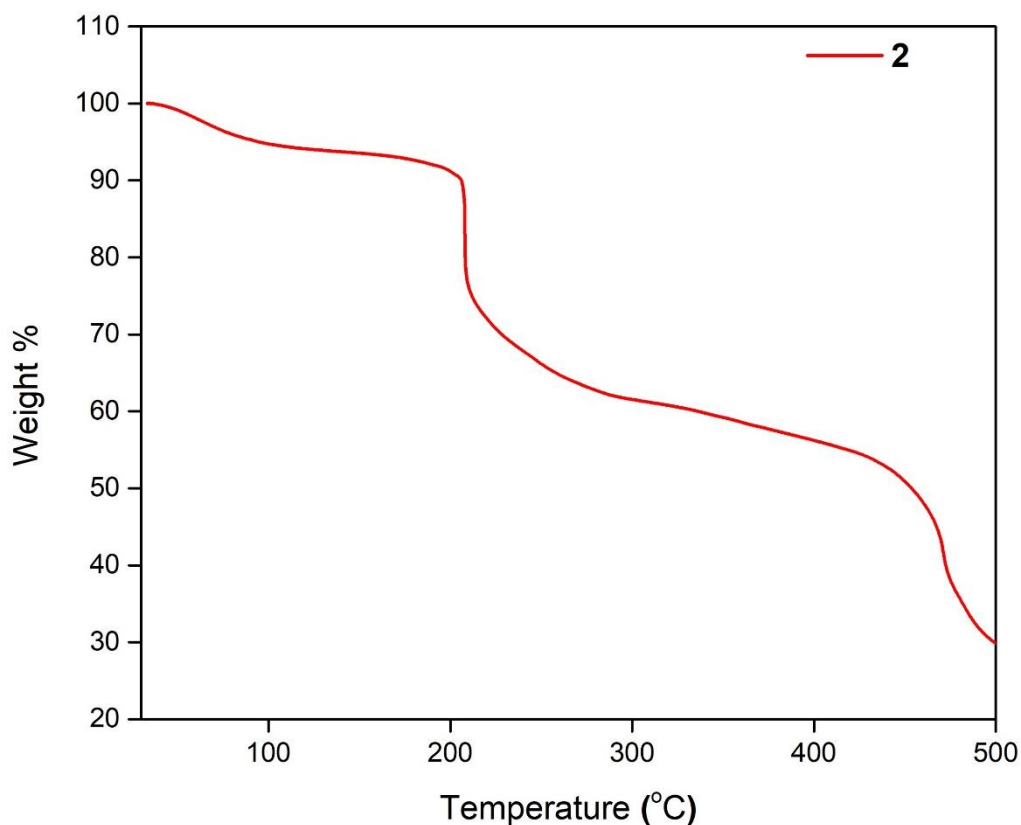**Figure 3.7.** TGA profile of $\{[Cu(L\text{-}HTyrbenz)_2]\cdot CH_3OH\cdot H_2O\}_n$.

Figure 3.8. TGA profile of $\{[Cu(L\text{-}HTyrthio)_2]\cdot H_2O\}_n$.

As the copper oxide nanoparticles are synthesized by the direct calcination of the copper metal complex precursor, the thermogravimetric study was performed to examine its decomposition behaviour. From the TGA behaviour of **1** and **2**, it is clear that complex gets almost fully decomposed by 500 °C. This information was further used for the calcination process of the precursor coordination polymers to produce CuO nanoparticles. Nonetheless, in the case of **2**, there can be the formation of CuS along with CuO as there is the presence of sulphur in the thiophene ring of the system.

1.2. Metal oxide nanoparticles

1.2.1. CuO-1

1.2.1.1. *Synthesis.* Through the top-down approach, these coordination polymers can act as sacrificial templates to obtain the nanomaterials with desired morphologies. Copper oxide nanoparticles were synthesized by the direct calcination of precursor coordination polymer **1** (Scheme 3.6.). The tube furnace was set for the below-mentioned heating and cooling program (Program A) after keeping the sample inside. The brownish-black powder

obtained after the calcination process was washed with double distilled water and methanol multiple times, followed by drying at 60 °C for 6 h to obtain the CuO nanoparticles. The obtained CuO nanoparticles were pure with an excellent yield of 75 %. There was no usage of any surfactants or chelating agents, and the process can be easily scaled up in order to produce CuO nanoparticles in higher amount.

Scheme 3.6. Synthesis of **CuO-1** from **1**

$$\{[Cu(L\text{-}HTyrbenz)_2]\cdot CH_3OH\cdot H_2O\}_n \xrightarrow{\text{Program A}} \text{CuO-1}$$

Program A
1) 30 °C - 550 °C, rate = 60 °C/h
2) 550 °C for 4 h
3) 550 °C - 30 °C, rate = 60 °C/h
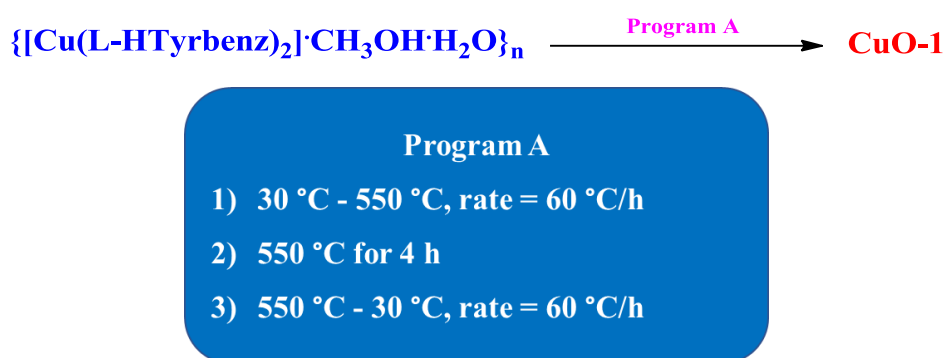
The optimization strategies followed for the synthesis of CuO nanoparticles from **1** through calcination method is described in Table 3.1. After a series of experiments, the appropriate time and temperature required for the formation of CuO nanoparticles from **1** was obtained and is 4 h and 550 °C.

Table 3.1. Optimization of the reaction conditions for the synthesis of **CuO-1**

Sl.No	Heating rate (°C/h)	Holding temperature (°C)	Holding time (h)	Results
1	60	550	1	No CuO formation
2	60	550	8	CuO formed Less yield
3	60	550	4	CuO formed Good yield

1.2.1.2. *Characterization.* The as-synthesized **CuO-1** were characterized by FT-IR spectroscopy, PXRD, FESEM and TEM techniques.

1.2.1.2.1. *FT-IR spectroscopy.* FT-IR spectrum was recorded in the solid-state as KBr pellet in the 400-4000 cm^{-1} range. FT-IR analysis (Figure 3.9) of as-synthesized CuO nanoparticles showed a strong band at 538 cm^{-1} which is due to Cu-O bond stretching, confirming the formation of CuO nanoparticles.[49] The peak at 3430 cm^{-1} can be due to the O-H stretching of the water molecules that are adsorbed to the CuO surface. Any peak corresponding to the precursor complex (**1**) is not observed in the spectrum and hence proving the purity of the as-synthesized **CuO-1**.
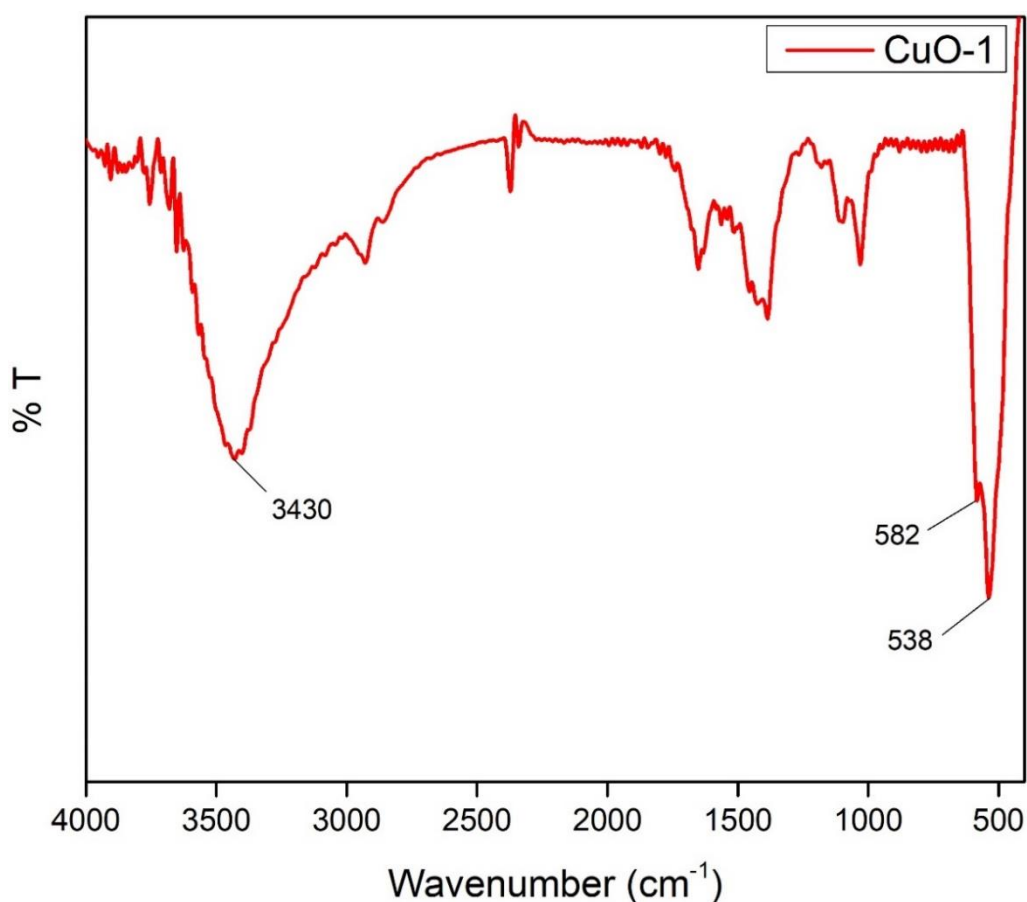

Figure 3.9. FT-IR spectrum of **CuO-1**.

1.2.1.2.2. *X-ray diffraction studies.* PXRD pattern of the as-prepared CuO nanoparticles is shown in Figure 3.10. The obtained patterns are in accordance with the standard patterns of the CuO (JCPDS No. 48-1548) having a monoclinic crystalline phase and *C*2/*c* space group. The peaks were sharp and clear, indicating the good crystallinity of the CuO

nanoparticles. Moreover, there was no presence of any extra peaks due to any other impurities, showing the high purity of the obtained nanostructures.

The XRD data were used to calculate the crystallite size of CuO particles. The Scherrer's formula[50] was used to determine the crystalline nature and the grain size of the as-synthesized CuO nanoparticles which is given by,

$$D = 0.9\lambda/\beta Cos\theta$$

where D is the grain size (nm), λ is the wavelength of the Cu Kα X-ray radiation (0.154nm), β is the line broadening at half the maximum intensity (FWHM) in radians, and θ is the Bragg's angle. The crystallite size of the CuO nanoparticles was calculated based on the peaks that were observed at different 2θ values in the PXRD pattern, and the average of these was considered. From the calculations, the average crystallite size of the synthesized CuO nanoparticles is found to be 60 nm
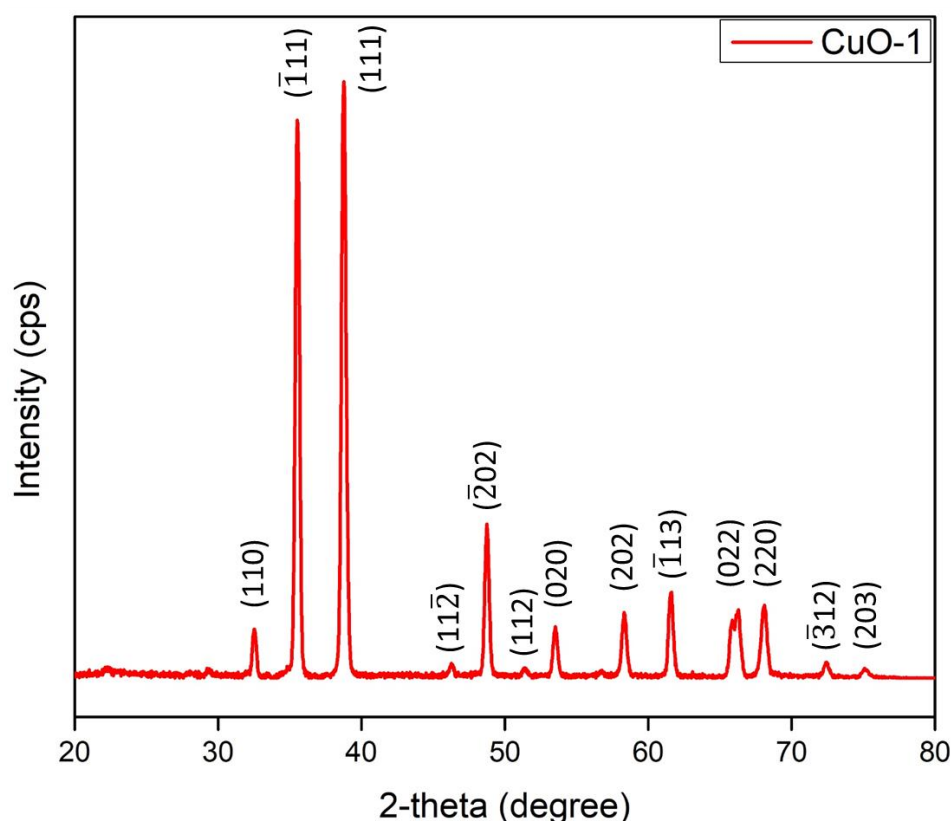

Figure 3.10. PXRD pattern of **CuO-1**.

1.2.1.2.3. *FESEM and EDX analysis.* Surface morphology of the as-synthesized **CuO-1** was determined using FESEM, as shown in Figure 3.11. For FESEM measurements, a uniform and fine dispersion of CuO slurry were prepared by taking ~1 mg of CuO

nanoparticle in a glass vial having 1 ml MeOH, followed by sonication for 30 min. Samples were drop casted at silicon wafer using a pipette, and the gold coating was done for 20 seconds. It was found that when plastic vials were used, the aggregation in the nanoparticle was quite higher.

The FESEM micrograph shows a uniform distribution of spherical nanoparticles throughout the sample. These spherical nanoparticles are aggregated to form porous microspheres. Furthermore, the sonication time had an effect on the aggregation of these nanoparticles. When sonication time was less, the aggregation of nanoparticles was very high, and it appeared as a lump. When the time was increased to 30 min, the spherical nanoparticles were sufficiently segregated enough to view their porous nature. Another insight into the purity of the as-synthesized CuO nanoparticles was studied through EDX analysis. From the EDX analysis (Figure 3.11), peaks for Cu and O was only visible confirming the result from PXRD analysis that the synthesized nanoparticles were of the purest form and no other impurities were present.
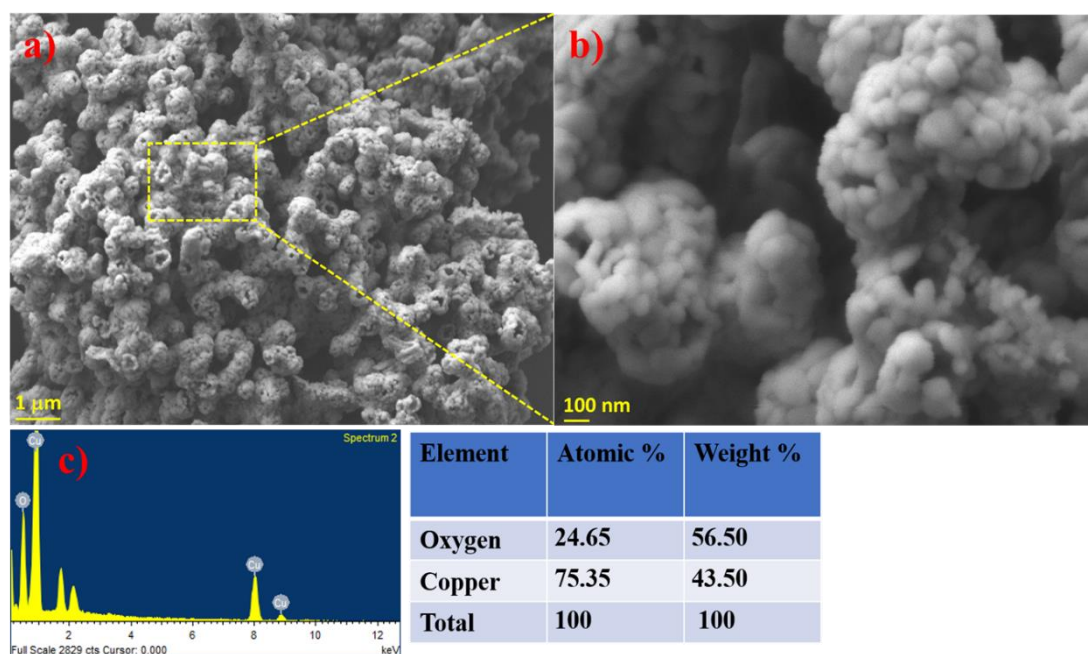

Element	Atomic %	Weight %
Oxygen	24.65	56.50
Copper	75.35	43.50
Total	100	100

Figure 3.11. a) and b) FESEM images of CuO nanoparticles c) EDX analysis of CuO nanoparticles.

1.2.1.2.4. *TEM analysis.* Surface morphology of the synthesized **CuO-1** was further analyzed using TEM, as shown in Figure 3.12. TEM analysis reveals similar results as that of FESEM, showing aggregated spherical CuO nanoparticles. The average size of the spherical nanoparticle is found to be 50 nm, which is in accordance with the results from

PXRD. Inset shows the SAED pattern of the CuO nanoparticle. The bright spots in the pattern further confirm the result that **CuO-1** is highly crystalline nature.
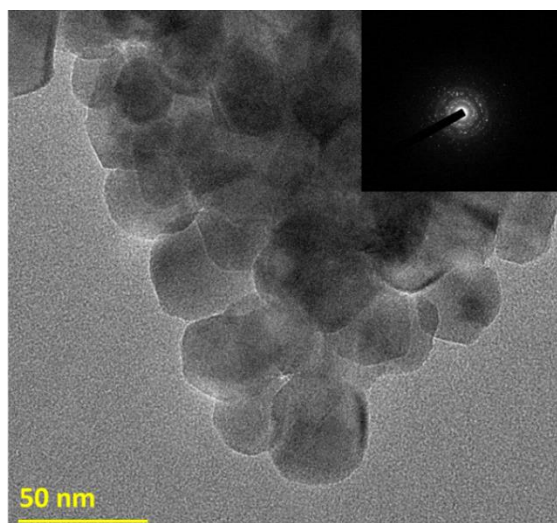

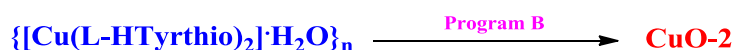**Figure 3. 12.** TEM images of **CuO-1**. (Inset shows the SAED pattern).

1.2.2. CuO-2

1.2.2.1. *Synthesis*. Copper oxide nanoparticles were synthesized by the direct calcination of precursor coordination polymer **2** (Scheme 3.7.). The tube furnace was set for the below-mentioned heating and cooling program (Program A) after keeping the sample inside. The brownish-black powder obtained after the calcination process was washed with double distilled water and methanol multiple times, followed by drying at 60 °C for 6 h to obtain the CuO nanoparticles. The obtained CuO nanoparticles were pure with an excellent yield of 75 %. There was no usage of any surfactants or chelating agents, and the process can be easily scaled up in order to produce CuO nanoparticles in higher amount.

The presence of sulphur in the thiophene ring of **2** resulted in the formation of CuS along with CuO. However, when temperature and time were further increased, the pure copper oxide was formed. It can be due to the conversion of as formed CuS into CuO as given in the equation below:

$$2CuS \ + \ 3O_2 \longrightarrow 2SO_2 \ + \ 2CuO$$
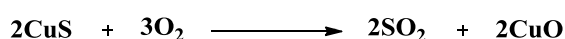
Scheme 3.7. Synthesis of **CuO-2** from **2**

$$\{[Cu(L\text{-}HTyrthio)_2]\cdot H_2O\}_n \xrightarrow{\text{Program B}} CuO\text{-}2$$

30

Table 3.2. Optimization of the reaction conditions for the synthesis of **CuO-2**.

Sl.No	Heating rate (°C/h)	Holding temperature (°C)	Holding time (h)	Results
1	60	550	4	No CuO formation
2	60	650	4	Mixture of CuS and CuO formed Less yield
3	60	800	6	Pure CuO formed Good yield

The optimization strategies followed for the synthesis of CuO nanoparticles from **2** through calcination method is detailed in Table 3.2. After a series of experiments, the appropriate time and temperature required for the formation of CuO nanoparticles from **2** was obtained and is 6 h and 850 °C.

1.2.2.2. *Characterization*. The as-synthesized **CuO-1** were characterized by FT-IR spectroscopy, PXRD, FESEM and TEM techniques.

1.2.2.2.1. *FT-IR spectroscopy.* FT-IR spectrum was recorded in the solid-state as KBr pellet in the 400-4000 cm^{-1} range. FT-IR analysis (Figure 3.13.) of as-synthesized CuO nanoparticles revealed a strong band at 618 cm^{-1} and 525 cm^{-1} which is due to the vibrations of Cu-O, confirming the formation of CuO nanoparticles.[51]
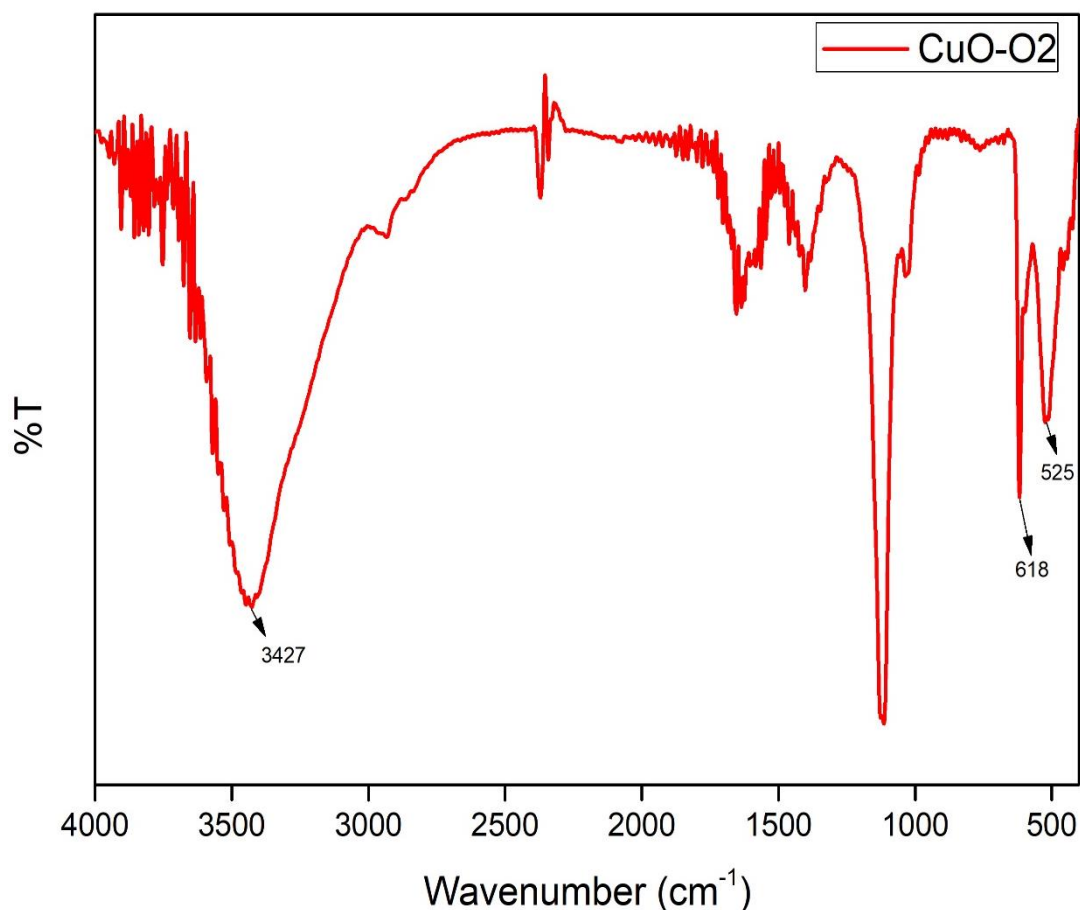
Figure 3.13. FT-IR spectrum of **CuO-2**.

1.2.2.2.2. *X-ray diffraction studies.* XRD pattern of as-prepared CuO nanoparticles is shown in Figure 3.14. The obtained patterns are in accordance with the standard patterns of the CuO (JCPDS No. 48-1548) having a monoclinic crystalline phase and *C*2/*c* space group. The peaks were sharp and clear, indicating the excellent crystallinity of the CuO nanoparticles. Furthermore, there was no presence of any extra peaks due to any other impurities, showing the high purity of the obtained nanostructures.

1.2.2.2.3. *FESEM and EDX analysis.* Surface morphology of the synthesized **CuO-2** was determined using FESEM is shown in Figure 3.15. For FESEM measurements, a uniform and fine dispersion of CuO slurry were prepared in MeOH. Samples were prepared at silicon wafer by drop cast method using a pipette, and the gold coating was done for 20 seconds. FESEM analysis shows the presence of rod-like shaped CuO nanostructures. The purity of the as-synthesized CuO nanoparticles was further confirmed by EDX analysis. From the EDX analysis (Figure 3.15), peaks for Cu and O was only visible confirming the result from PXRD analysis that the synthesized nanoparticles were of the purest form and no other impurities were present.
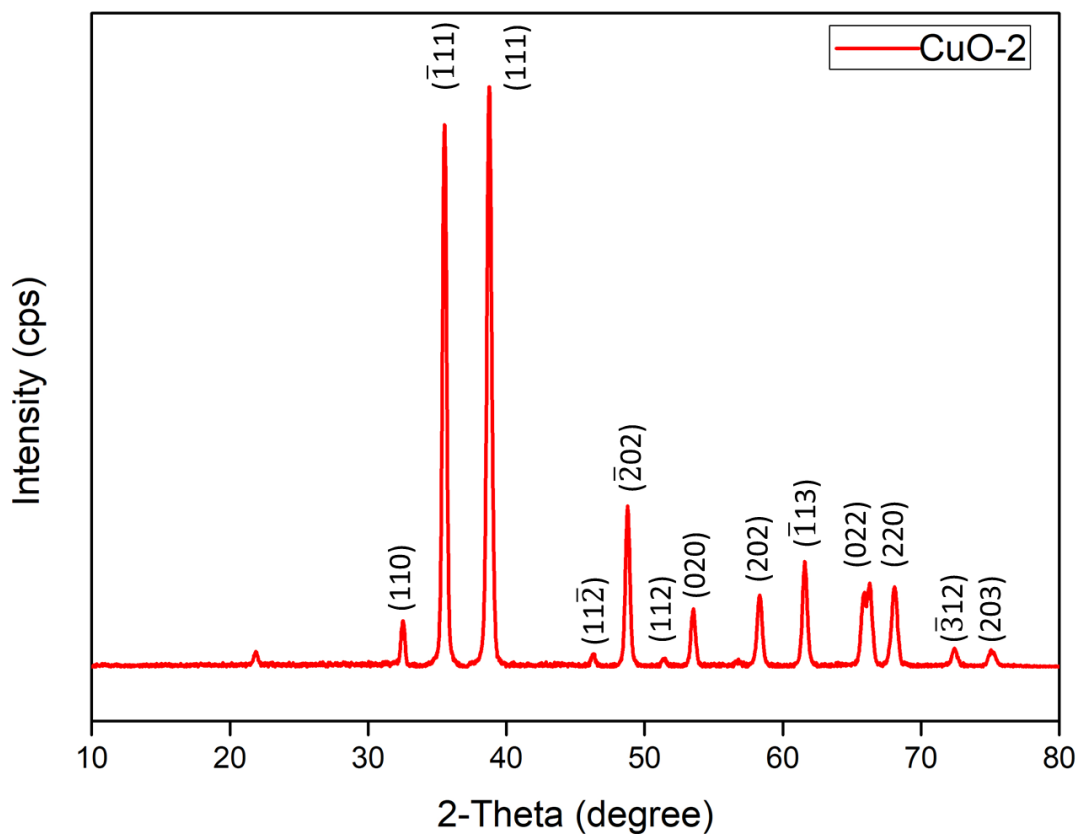
Figure 3.14. PXRD pattern of **CuO-2**.
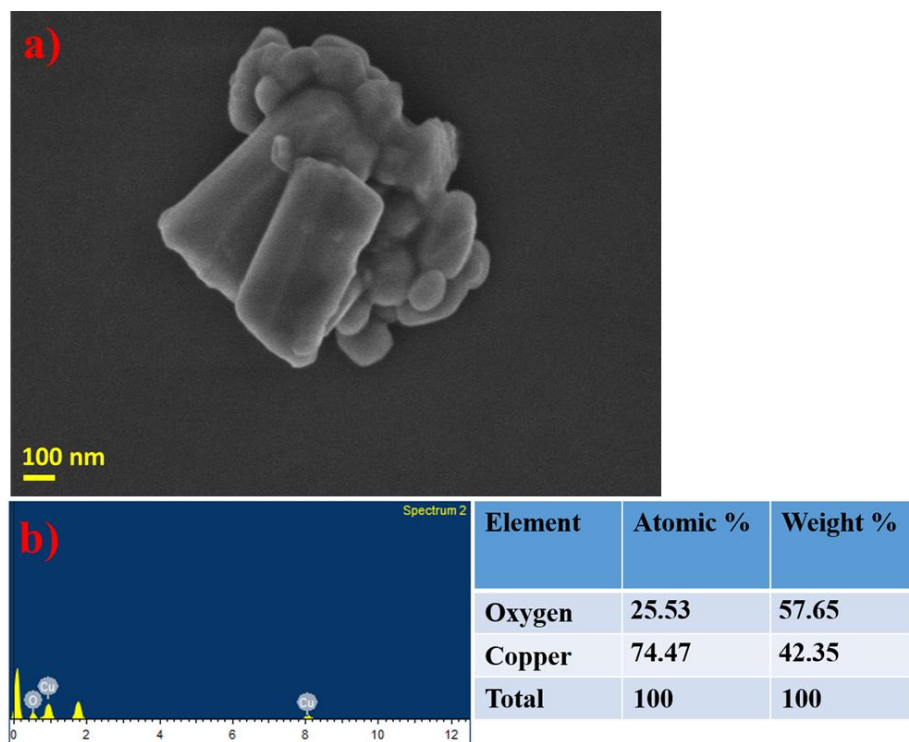

Element	Atomic %	Weight %
Oxygen	25.53	57.65
Copper	74.47	42.35
Total	100	100

Figure 3.15. a) FESEM images of CuO nanoparticles b) EDX analysis of CuO nanoparticles.

1.2.2.2.4. *TEM analysis.* Surface morphology of the synthesized **CuO-2** was further analyzed using TEM, as shown in Figure 3.16. TEM analysis reveals similar results as that of FESEM, showing rod-shaped CuO nanoparticles. Inset shows the SAED pattern of the CuO nanoparticle. The bright spots in the pattern further confirm the result that **CuO-2** is highly crystalline in nature.
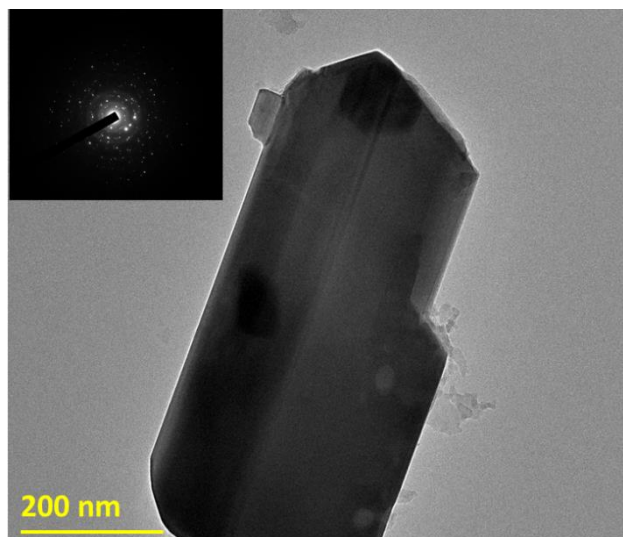

Figure 3.16. TEM images of **CuO-2**.

2. Temperature-dependent study of the formation of CuO-1

It is reported that the annealing temperature has an important role in the resulting morphology of metal oxide nanostructures.[52–58] CuO nanostructures were fabricated under different temperature in order to study the temperature effect. The fabrication was carried by following the standard procedure for preparing CuO from **1** reported in the experimental section, except the annealing temperature. **1** was calcined at 550 °C, 700 °C, and 800 °C to synthesize CuO nanostructures. The morphology of the as-prepared CuO nanostructures was different, in consistence with expected dependency in temperature in the fabrication of CuO nanostructures with different morphology.

2.1. *X-ray diffraction studies*. The diffraction patterns of the CuO nanostructures synthesized at different temperatures were determined in order to find the crystalline phase of the as-prepared nanostructures. The PXRD pattern (Figure 3.17) obtained were in good agreement with the standard JCPDS data for the CuO. (JCPDS No. 48-1548) All the three CuO nanostructures contained only monoclinic structure as the crystallographic phase, and the peaks were sharp and clear peaks indicating the excellent crystallinity of the CuO

nanostructures. Furthermore, there was no presence of any extra peaks due to any other impurities, showing the high purity of the obtained nanostructures.
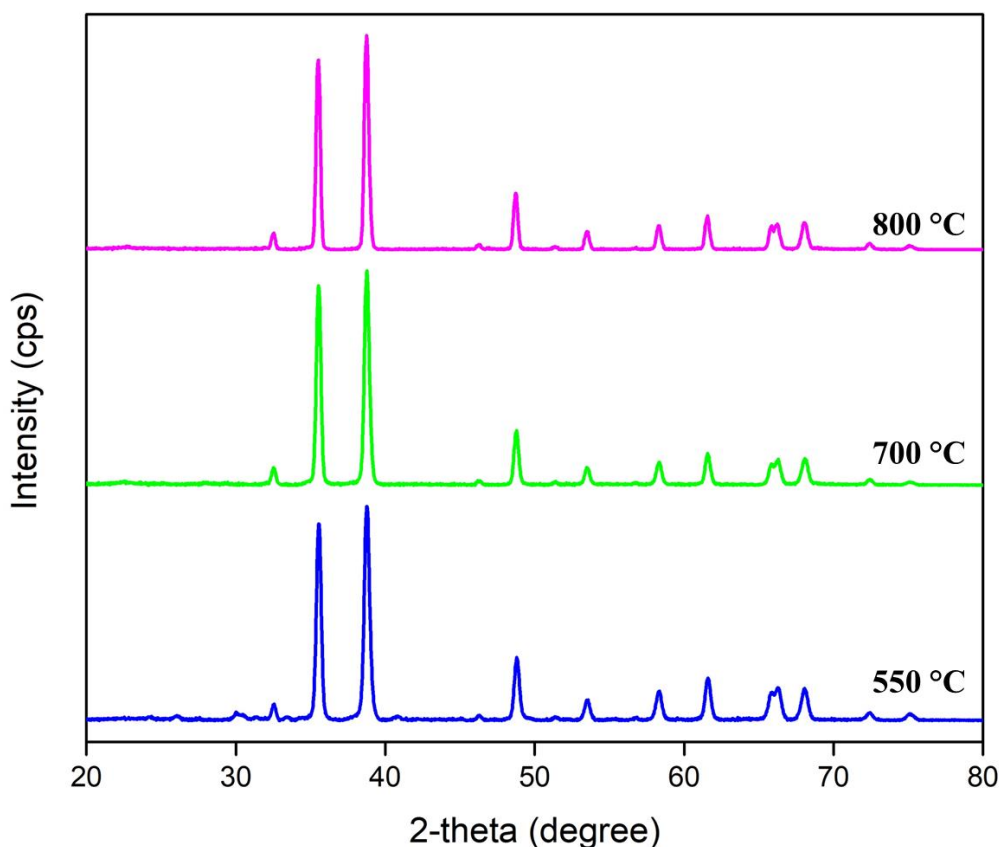

Figure 3.17. PXRD pattern of CuO nanostructures formed at 550 °C, 700 °C and 800 °C.

2.2. *Surface Analysis*. The morphology of the as-prepared CuO nanostructures was studied using FESEM and TEM (Figure 3.18). When **1** was calcined at 550 °C, spherical CuO nanoparticles were formed which aggregated to form porous spherical structures, as confirmed from the FESEM and TEM images. On further increasing the annealing temperature to 700 °C, rod shape CuO structures were formed. Furthermore, heating at 800 °C produced cubic shaped nanostructures.

Thus, a morphological transformation from spherical to the rod to cubic shaped nanostructures were observed for CuO, upon varying the annealing temperature. Hence, the study confirmed that temperature has a significant effect in determining the morphology of CuO nanostructures.
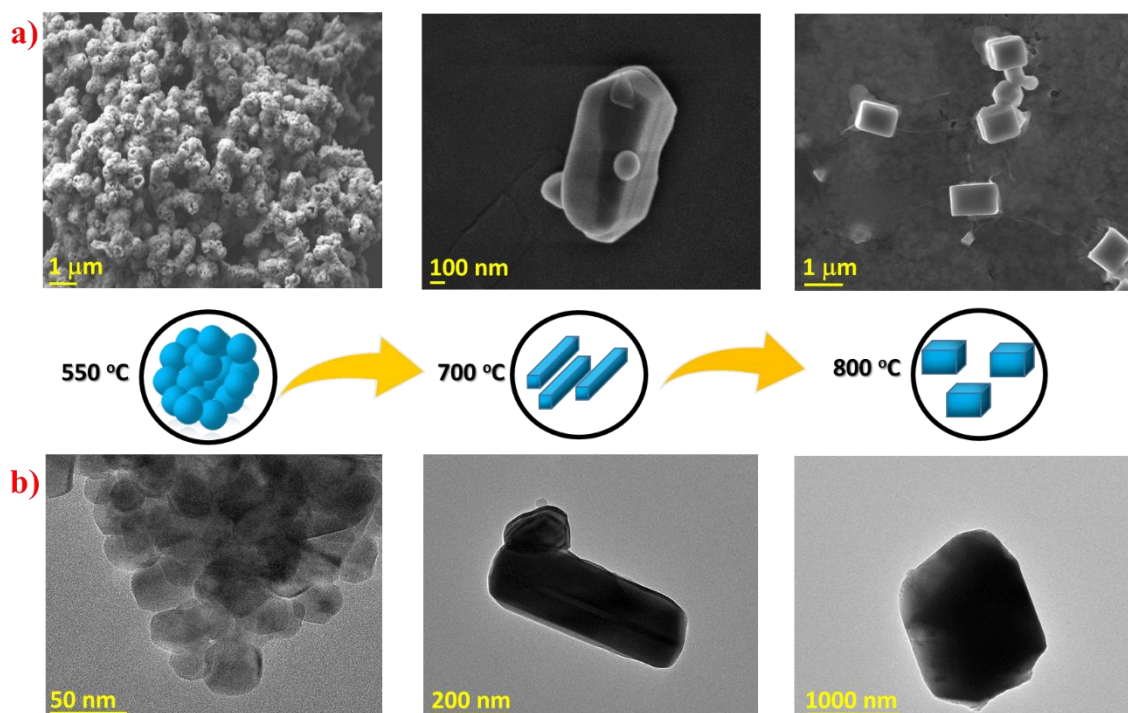
Figure 3.18. a) FESEM and b) TEM images showing the morphological transformation.

A plausible growth mechanism is proposed for the transformation of CuO nanostructures from spherical to the rod to cubic shapes (Scheme 3.8). First of all, the nucleation growth of the crystals takes place to form seed crystals. This seed crystals further grows to form the initial spherical nanostructures. The stability of atoms in a nanoparticle decreases simultaneously with the decrease in particle size due to the increase in surface energy.[59,60] In the case of spherical nanoparticles, they are composed of high-order unstable facets such as {>1,>1,>1} with high surface energies[61]. The total surface area of such unstable facets increases conjointly with the decrease in particle size. Therefore, these unstable atoms in a small spherical nanoparticle can be released, allowing further movement into another nanoparticle. Thus, a wide range of atom transportation is happening among nanoparticles. This atom transportation can result in the morphological transformation of the nanoparticles into stable morphologies such as cubes with low surface-energy facets {100} or into to the agglomeration of spheres. The energy for this transformation is provided in the form of thermal energy, which increases upon increasing temperature. Moreover, the increase in the temperature can result in an increased surface activity of the particles, which can result in morphological transformation.[62]

Scheme 3.8. A plausible mechanism of morphological transformation of **CuO-1**
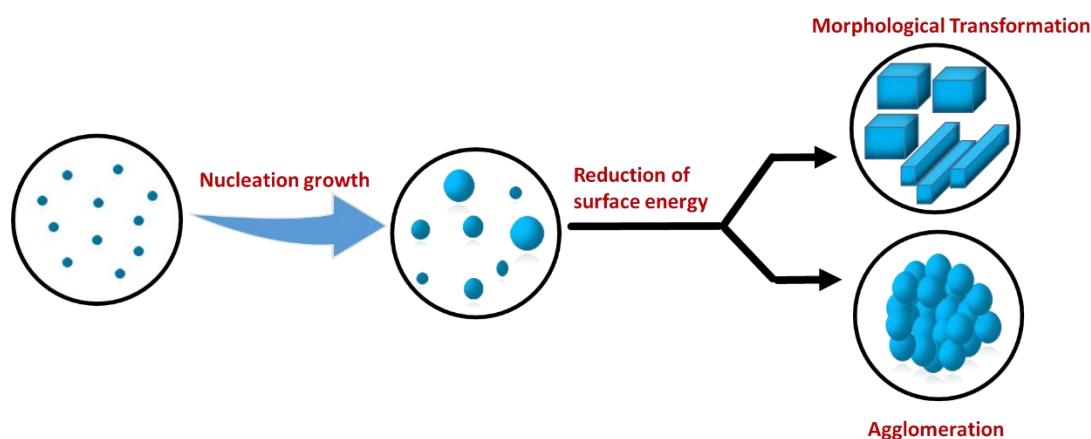
3. Catalytic studies

Catalysis has a critical role in science and industry due to their uses in numerous chemical transformations enclosing the fields of petrochemistry, pharmaceuticals, transportation, environmental remediation, among others.[63–66] Lewis acid catalysis is reactions where the catalyst, a Lewis acid, acts as an electron pair acceptor and thereby increasing the reactivity of the substrate. Lewis acid catalysts are mainly based on main group metals like aluminium[67], boron[68], tin[69], etc. and late and early transition metals like copper[70], iron[71], zirconium[72], titanium[73], etc. Among the numerous catalysts, those based on metal nanoparticles has achieved particular importance due to their remarkable chemical, electronic, and optical properties.[74–76] α-aminonitriles are interesting bifunctional compounds which are considered as the prebiotic precursors for porphyrins, nicotinic acids, nucleic acids, and corrins.[77–81] Strecker reaction, introduced by Adolf Strecker in 1850, after getting modified over decades, has now become three-component reaction with the most straightforward and efficient route for the synthesis of α-aminonitriles.[82]
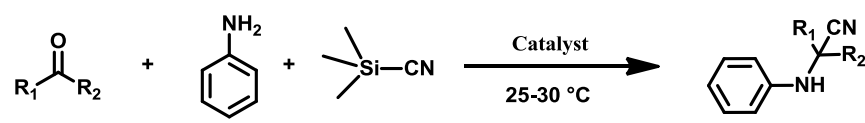
Due to the presence of an unsaturated metal center in **CuO-1**, their active role as a heterogeneous catalyst in Lewis acid promoted reactions have been studied. As α-aminonitriles acts as crucial intermediates in the synthetic procedure of various pharmaceutical products (e.g., saframycin A, ecteinascidin, 743, and phthalascidin) and peptides[73–78], their synthesis through Strecker reaction has got significant interest. Here, we have studied the catalytic activity of as-synthesized CuO nanoparticles in the one-pot, three-component Strecker reaction.
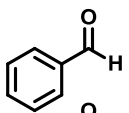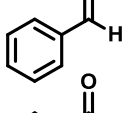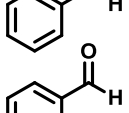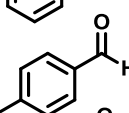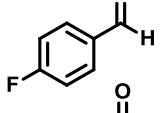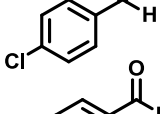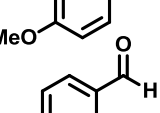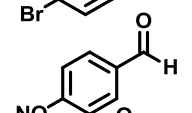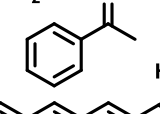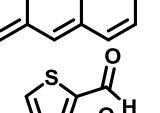
In order to check the efficiency of **CuO-1** in catalyzing Strecker reaction, we began with the simplest aldehyde, benzaldehyde, TMSCN, and aniline as substrates. After adding these substrates into a Schlenk tube, followed by a catalytic amount of activated **CuO-1**, the reaction was carried out in a solvent-free state at room temperature under a dinitrogen atmosphere. The progress of the reaction was monitored by TLC analysis, and the yield obtained was calculated using ^{1}H NMR spectroscopy. Further, the catalytic activity of **CuO-1** was tested for different substrates, including ketones and aldehydes. A time-dependent study of the catalysis was also carried out in the presence of **CuO-1**. The results of the reaction are summarised in Table 3.3.

The catalytic activity of **CuO-1** when benzaldehyde was used was quite high, having a yield of 94 %. Yield increased when the reaction time was increased from 1 h to 2 h, 3 h, 4 h, and 6 h. However, the increase in yield when time increased from 1h to 6h was only 6%, which is not a considerable increase. Further, under the optimized reaction conditions, a number of substrates containing electron-donating groups and electron-withdrawing groups attached to them were efficiently catalyzed by **CuO-1** in Strecker reaction; however, no significant electronic effect was observed.

Catalyst stability was checked by using its efficiency in reusability. To regenerate the active catalyst, it was filtered off, followed by washing with dichloromethane multiple times, and dried at 60 °C for 6 h. The regenerated catalyst was used for reusability study using the model reaction having benzaldehyde as substrate, keeping the reaction conditions unaltered. To check the stability of the regenerated catalyst, the spent catalyst was extensively characterized by PXRD, FESEM analyses and FT-IR spe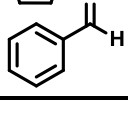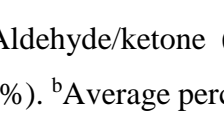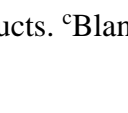ctroscopy. In both cases, it is clear from the PXRD patterns (Figure 3.19) of the recovered catalyst that, even after three, there is no loss of crystallinity or phase purity of the catalyst. Moreover, no morphological changes were observed during the recyclability for the catalyst shown from the FESEM images (Figure 3.20). In addition, the catalyst can be reused up to three successive runs with a loss of ~2−4 % in its catalytic activity, a loss which is negligible. The performance of the recycled catalyst in Strecker reaction up to three successive runs is shown in Figure 3.21. Furthermore, it was found from the FT-IR spectra that, there was a shift in the carbonyl stretching of the benzaldehyde, clearly showing the interaction between the metal center from the catalyst and carbonyl group (Figure 3.22).

Table 3.3. Optimization conditions and substrate scope for the Strecker reaction catalyzed by **CuO-1**[a]

Entry	Aldehyde/ketone	Time (h)	Yield[b] (%)
1	benzaldehyde	4	98
2	benzaldehyde	3	97
3	benzaldehyde	2	96
4	benzaldehyde	1	94
5	4-methylbenzaldehyde	1	97
6	4-fluorobenzaldehyde	1	97
7	4-chlorobenzaldehyde	1	95
8	4-methoxybenzaldehyde	1	96
9	4-bromobenzaldehyde	1	91
10	4-nitrobenzaldehyde	1	98
11	acetophenone	1	95
12	anthracene-2-carbaldehyde	1	70
13	thiophene-2-carbaldehyde	1	78
14	benzaldehyde	1	26[c]

Reaction conditions: Aldehyde/ketone (0.1 mmol), amine (0.1 mmol), TMSCN (0.12 mmol), catalyst (6 mol %). [b]Average percent yield for a set of triplicate runs, calculated by ^{1}H NMR of the crude products. [c]Blank reaction.
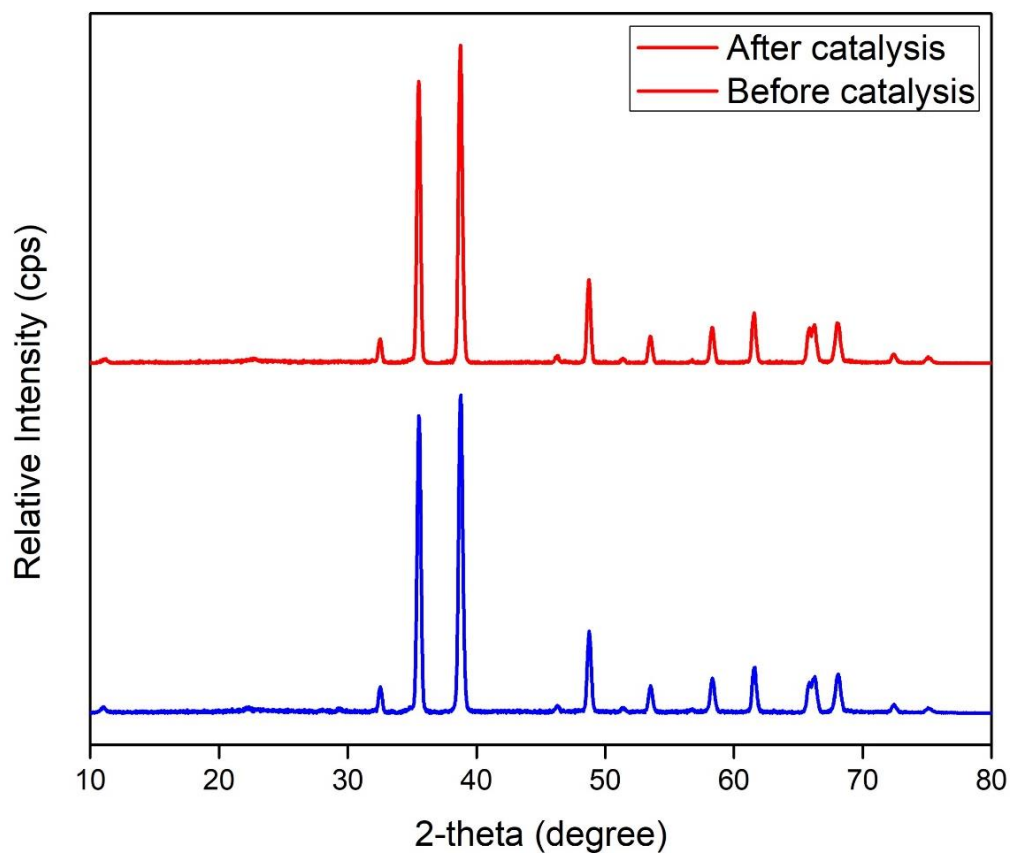
Figure 3.19. PXRD pattern of **CuO-1** before and after catalysis.
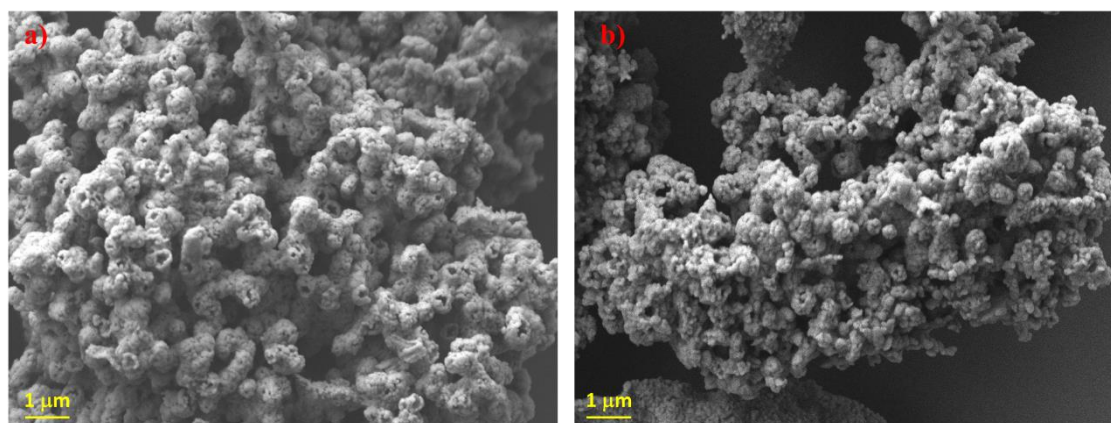
Figure 3.20. FESEM images of **CuO-1** before and after catalysis.
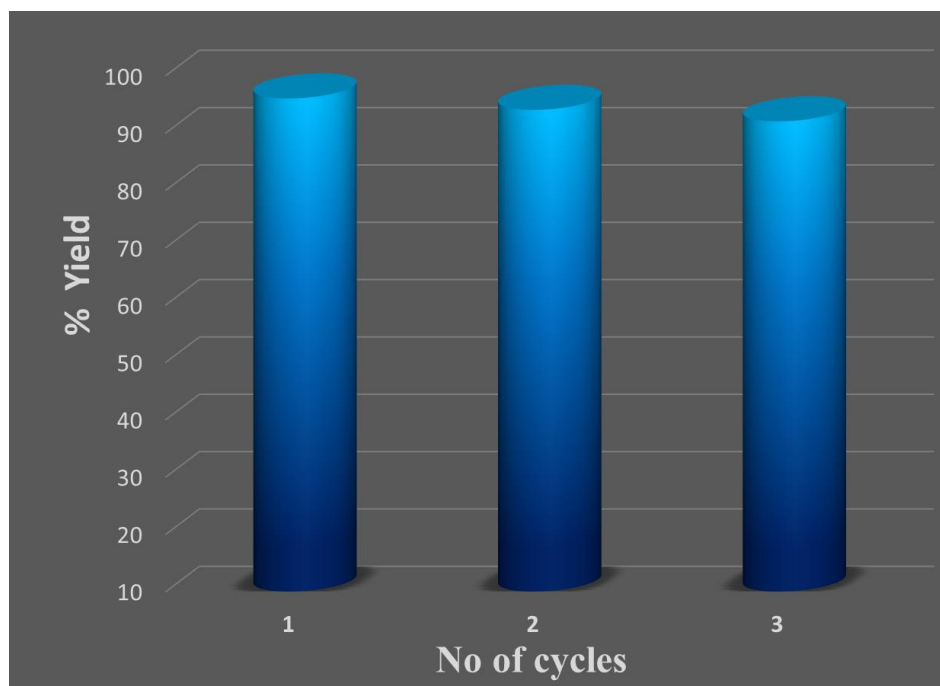
Figure 3.21. % yield for three consecutive cycles of the Strecker reaction of benzaldehyde with aniline and trimethylsilyl cyanide catalyzed by **CuO-1**.
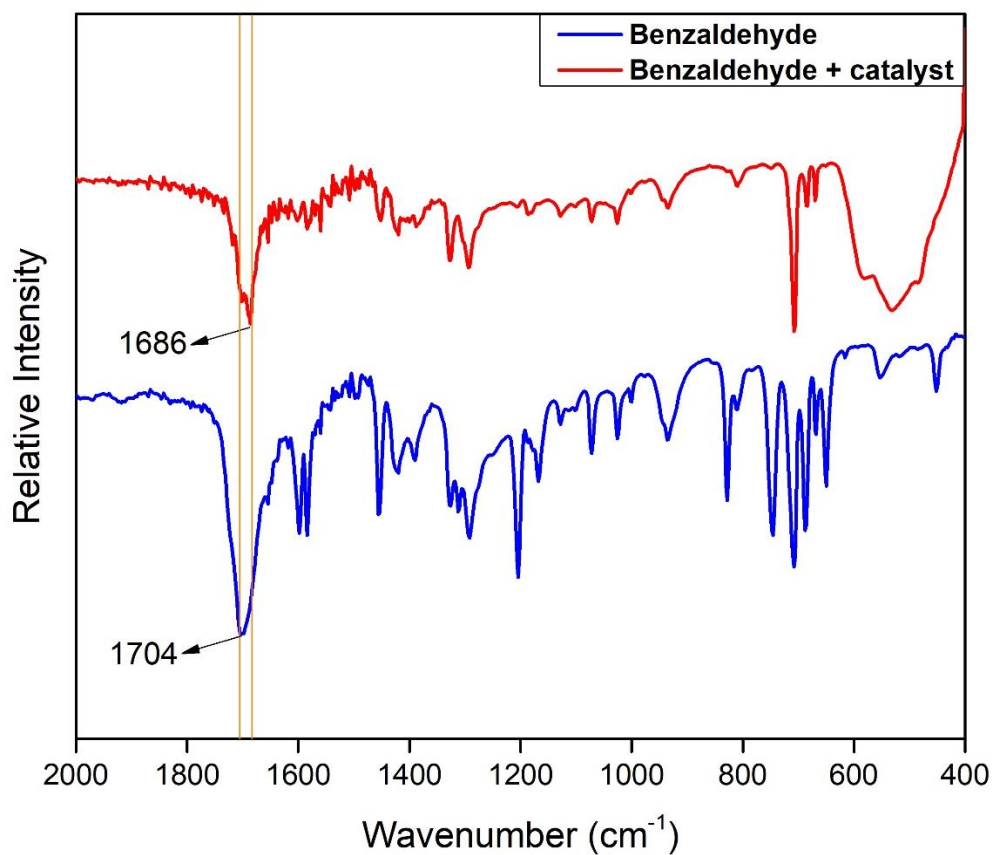
Figure 3.22. FT-IR spectra of free benzaldehyde and benzaldehyde with catalyst.

From the information gathered, a plausible mechanism for the reaction catalyzed by **CuO-1** is presented in Figure 3.23. The Lewis acidic metal center, copper, of **CuO-1** interacts with the oxygen of carbonyl groups and nitrogen of amino groups leading to the polarisation of these groups. Thus, this interaction facilitates the formation of imine intermediate and increases the electrophilic nature of the carbon atom of carbonyl or imine moiety. **CuO-1** further interacts with TMSCN to release the cyanide group, which upon having a nucleophilic addition reaction with imine gives the desired product.
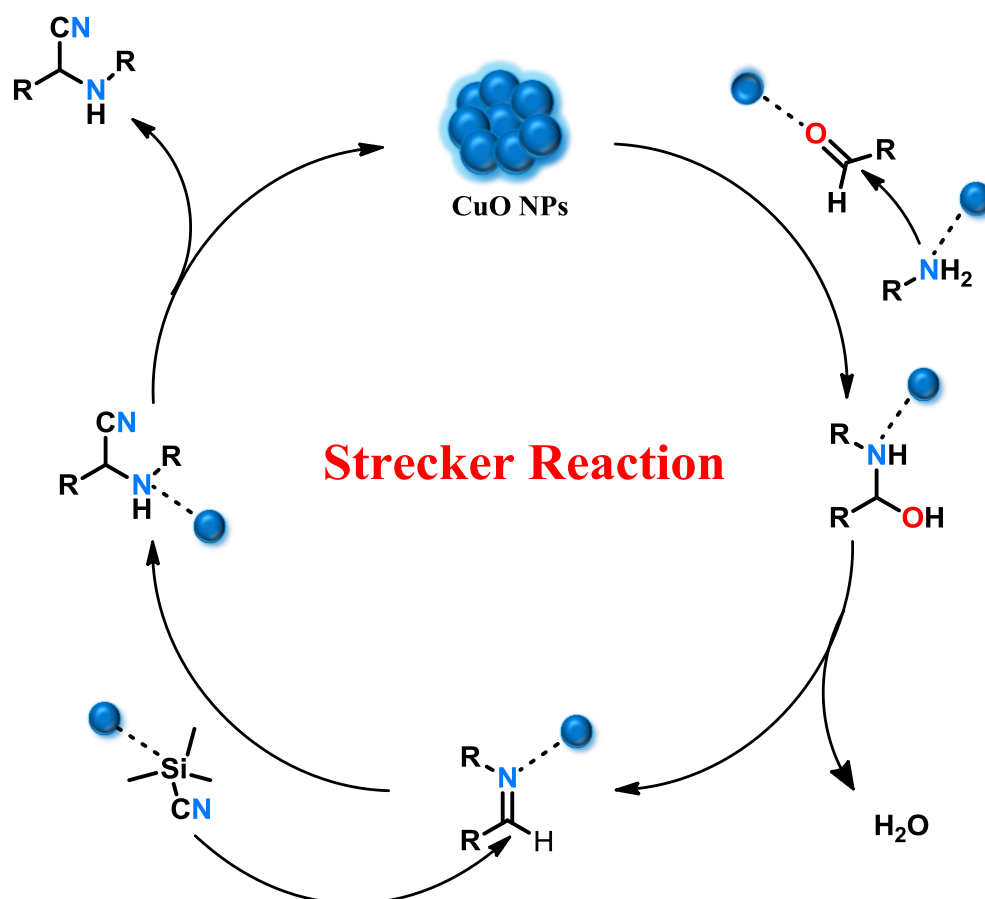
Figure 3.23. A plausible mechanism for the Strecker reaction catalyzed by **CuO-1**.

CHAPTER IV

CONCLUSIONS

In summary, two chiral amino acid ligands based coordination polymers, {[Cu(L-HTyrbenz)$_2$]·CH$_3$OH·H$_2$O}$_n$ (**1**) and {[Cu(L-HTyrthio)$_2$]·H$_2$O}$_n$ (**2**), were synthesized as the precursors for the formation of CuO nanoparticles. CuO nanoparticles were synthesized by a simple, efficient, cost-effective and high yield utilizing direct-calcination method under template-free and surfactant-less conditions. The uniformity in morphology and composition of CuO was obtained by optimization of parameters like time and temperature during calcination. The as-synthesized CPs and nanoparticles were well characterized by different techniques, such as FTIR, PXRD, FESEM and TEM analyses.

Temperature dependant morphology study for the formation of **CuO-1** was studied. A morphological transformation from spherical to rod and to cubic-shaped nanostructures was observed for CuO, upon varying the annealing temperature from 550 °C to 700 °C to 800 °C, respectively. Hence, the study confirmed that temperature has a significant role in determining the morphology of CuO nanostructures

The presence of an unsaturated metal centre and the large surface to volume ratio in the CuO nanoparticles have been utilized for catalytic activity toward the Lewis acid-catalyzed C-N bond-forming Strecker reaction. By optimizing the reaction conditions, it has been established that the CP derived CuO nanoparticle exhibit excellent catalytic efficiency under solvent-free condition (in the solid-state) at a very fast reaction rate. The structural and morphological stability of the catalyst during the reaction was retained and thus provided its heterogeneous nature. Furthermore, the catalyst can be easily separated and reused for three catalytic cycles without significant loss of its activity in both cases.

Thus, CPs derived copper oxide nanoparticles can be beneficially utilized in chemical industries as an excellent catalyst for synthesizing organic molecules of biological importance with enhanced productivity and a reduced amount of chemical waste at low cost. Copper oxide being a semiconductor with a narrow bandgap of ~1.2 eV, bandgap

properties of diverse CuO can be studied as the function of morphology and can be further used for applications like dye degradation under visible light. After being recognized as antimicrobial materials by the US Environmental Protection Agency (EPA), nanoparticles of copper and its oxides have received much attention to be used in biomedical devices to prevent bacterial infection. Thus, CPs derived copper oxide nanoparticles can also be studied for their antibacterial properties.

Nanotechnology and nanomaterials are the critical factors for a clean and sustainable future, and henceforth, the focus of research in these areas is a necessity. Thus, the current research should be concentrated in a way that it will benefit not only the humankind but also the mother earth.

BIBLIOGRAPHY

(1)   Kolahalam, L. A.; Kasi Viswanath, I. V.; Diwakar, B. S.; Govindh, B.; Reddy, V.; Murthy, Y. L. N. Review on Nanomaterials: Synthesis and Applications. *Materials Today: Proceedings* **2019**, *18*, 2182–2190.

(2)   Li, N.; Zhao, P.; Astruc, D. Anisotropic Gold Nanoparticles: Synthesis, Properties, Applications, and Toxicity. *Angewandte Chemie International Edition* **2014**, *53* (7), 1756–1789.

(3)   Filipponi, L.; Sutherland, D. S. Nanotechnologies : Principles, Applications, Implications and Hands-on Activities : A Compendium for Educators; 2012.

(4)   Burda, C.; Chen, X.; Narayanan, R.; El-Sayed, M. A. Chemistry and Properties of Nanocrystals of Different Shapes. *Chem. Rev.* **2005**, *105* (4), 1025–1102.

(5)   Guzelian, A. A.; Katari, J. E. B.; Kadavanich, A. V.; Banin, U.; Hamad, K.; Juban, E.; Alivisatos, A. P.; Wolters, R. H.; Arnold, C. C.; Heath, J. R. Synthesis of Size-Selected, Surface-Passivated InP Nanocrystals. *J. Phys. Chem.* **1996**, *100* (17), 7212–7219.

(6)   Henglein, A. Small-Particle Research: Physicochemical Properties of Extremely Small Colloidal Metal and Semiconductor Particles. *Chem. Rev.* **1989**, *89* (8), 1861–1873.

(7)   Schüth, F.; Sing, K. S. W.; Weitkamp, J. *Handbook of Porous Solids*; Wiley-VCH: Weinheim, Germany, 2002.

(8)   Kitagawa, S.; Kitaura, R.; Noro, S. Functional Porous Coordination Polymers. *Angewandte Chemie International Edition* **2004**, *43* (18), 2334–2375.

(9)   Heitbaum, M.; Glorius, F.; Escher, I. Asymmetric Heterogeneous Catalysis. *Angewandte Chemie International Edition* **2006**, *45* (29), 4732–4762.

(10)   Bayda, S.; Adeel, M.; Tuccinardi, T.; Cordani, M.; Rizzolio, F. The History of Nanoscience and Nanotechnology: From Chemical–Physical Applications to Nanomedicine. *Molecules* **2020**, *25* (1), 112.

(11)   Cho, E. J.; Holback, H.; Liu, K. C.; Abouelmagd, S. A.; Park, J.; Yeo, Y. Nanoparticle Characterization: State of the Art, Challenges, and Emerging Technologies. *Mol. Pharmaceutics* **2013**, *10* (6), 2093–2110.

(12)   Mary Ealias, A.; M P, S. A Review on the Classification, Characterization, Synthesis of Nanoparticles and Their Application. *IOP Conference Series Materials Science and Engineering* **2017**, *263*, 032019.

(13)   K. Sharma, V.; Filip, J.; Zboril, R.; S. Varma, R. Natural Inorganic Nanoparticles – Formation, Fate, and Toxicity in the Environment. *Chemical Society Reviews* **2015**, *44* (23), 8410–8423.

(14)   Bhaviripudi, S.; Mile, E.; Steiner, S. A.; Zare, A. T.; Dresselhaus, M. S.; Belcher, A. M.; Kong, J. CVD Synthesis of Single-Walled Carbon Nanotubes from Gold Nanoparticle Catalysts. *J. Am. Chem. Soc.* **2007**, *129* (6), 1516–1517.

(15)   Komarneni, S. Feature Article. Nanocomposites. *J. Mater. Chem.* **1992**, *2* (12), 1219–1230.

(16)   Astruc, D.; Chardac, F. Dendritic Catalysts and Dendrimers in Catalysis. *Chem. Rev.* **2001**, *101* (9), 2991–3024.

(17)   Salavati-Niasari, M.; Davar, F.; Mir, N. Synthesis and Characterization of Metallic Copper Nanoparticles via Thermal Decomposition. *Polyhedron* **2008**, *27* (17), 3514–3518.

(18) Tai, C. Y.; Tai, C.-T.; Chang, M.-H.; Liu, H.-S. Synthesis of Magnesium Hydroxide and Oxide Nanoparticles Using a Spinning Disk Reactor. *Ind. Eng. Chem. Res.* **2007**, *46* (17), 5536–5541.

(19) Poh, T. Y.; Ali, N. A. B. M.; Mac Aogáin, M.; Kathawala, M. H.; Setyawati, M. I.; Ng, K. W.; Chotirmall, S. H. Inhaled Nanomaterials and the Respiratory Microbiome: Clinical, Immunological and Toxicological Perspectives. *Particle and Fibre Toxicology* **2018**, *15* (1), 46.

(20) Rawat, R. S. Dense Plasma Focus - From Alternative Fusion Source to Versatile High Energy Density Plasma Source for Plasma Nanotechnology. *J. Phys.: Conf. Ser.* **2015**, *591*, 012021.

(21) Salah, N.; Habib, S. S.; Khan, Z. H.; Memic, A.; Azam, A.; Alarfaj, E.; Zahed, N.; Al-Hamedi, S. High-Energy Ball Milling Technique for ZnO Nanoparticles as Antibacterial Material. *Int J Nanomedicine* **2011**, *6*, 863–869.

(22) Vieu, C.; Carcenac, F.; Pépin, A.; Chen, Y.; Mejias, M.; Lebib, A.; Manin-Ferlazzo, L.; Couraud, L.; Launois, H. Electron Beam Lithography: Resolution Limits and Applications. *Applied Surface Science* **2000**, *164*, 111–117.

(23) Zheng, F.; Lu, H.; Guo, M.; Zhang, M.; Zhen, Q. Hydrothermal Preparation of WO3 Nanorod Array and ZnO Nanosheet Array Composite Structures on FTO Substrates with Enhanced Photocatalytic Properties. *J. Mater. Chem. C* **2015**, *3* (29), 7612–7620.

(24) Kammler, H. K.; Mädler, L.; Pratsinis, S. E. Flame Synthesis of Nanoparticles. *Chemical Engineering & Technology* **2001**, *24* (6), 583–596.

(25) Borsella, E.; D'Amato, R.; Terranova, G.; Falconieri, M.; Fabbri, F. Synthesis of Nanoparticles by Laser Pyrolysis: From Research to Applications. *Energia, Ambiente e Innovazione* **2011**, *4*, 54–64.

(26) Amendola, V.; Meneghetti, M. Laser Ablation Synthesis in Solution and Size Manipulation of Noble Metal Nanoparticles. *Phys. Chem. Chem. Phys.* **2009**, *11* (20), 3805–3821.

(27) Verma, N.; Kumar, N. Synthesis and Biomedical Applications of Copper Oxide Nanoparticles: An Expanding Horizon. *ACS Biomater. Sci. Eng.* **2019**, *5* (3), 1170–1188.

(28) Kim, I.-D.; Rothschild, A.; Lee, B. H.; Kim, D. Y.; Jo, S. M.; Tuller, H. L. Ultrasensitive Chemiresistors Based on Electrospun TiO_2 Nanofibers. *Nano Lett.* **2006**, *6* (9), 2009–2013.

(29) Brovelli, S.; Chiodini, N.; Lorenzi, R.; Lauria, A.; Romagnoli, M.; Paleari, A. Fully Inorganic Oxide-in-Oxide Ultraviolet Nanocrystal Light Emitting Devices. *Nature Communications* **2012**, *3* (1), 690.

(30) Stein, A. Batteries Take Charge. *Nature Nanotech* **2011**, *6* (5), 262–263.

(31) Amini, M.; Naslhajian, H.; Farnia, S. M. F.; Kang, H. K.; Gautam, S.; Chae, K. H. Polyoxomolybdate-Stabilized Cu_2O Nanoparticles as an Efficient Catalyst for the Azide–Alkyne Cycloaddition. *New J. Chem.* **2016**, *40* (6), 5313–5317.

(32) Deka, P.; Deka, R. C.; Bharali, P. Porous CuO Nanostructure as a Reusable Catalyst for Oxidative Degradation of Organic Water Pollutants. *New J. Chem.* **2016**, *40* (1), 348–357.

(33) Deka, P.; Hazarika, A.; Deka, R. C.; Bharali, P. Influence of CuO Morphology on the Enhanced Catalytic Degradation of Methylene Blue and Methyl Orange. *RSC Adv.* **2016**, *6* (97), 95292–95305.

(34) Giri, S. D.; Sarkar, A. Electrochemical Study of Bulk and Monolayer Copper in Alkaline Solution. *J. Electrochem. Soc.* **2016**, *163* (3), H252.

(35)   Khan, R.; Ahmad, R.; Rai, P.; Jang, L.-W.; Yun, J.-H.; Yu, Y.-T.; Hahn, Y.-B.; Lee, I.-H. Glucose-Assisted Synthesis of Cu_2O Shuriken-like Nanostructures and Their Application as Nonenzymatic Glucose Biosensors. *Sensors and Actuators B: Chemical* **2014**, *203*, 471–476.

(36)   Zhong, Z.; Ng, V.; Luo, J.; Teh, S.-P.; Teo, J.; Gedanken, A. Manipulating the Self-Assembling Process to Obtain Control over the Morphologies of Copper Oxide in Hydrothermal Synthesis and Creating Pores in the Oxide Architecture. *Langmuir* **2007**, *23* (11), 5971–5977.

(37)   Vijaya Kumar, R.; Elgamiel, R.; Diamant, Y.; Gedanken, A.; Norwig, J. Sonochemical Preparation and Characterization of Nanocrystalline Copper Oxide Embedded in Poly(Vinyl Alcohol) and Its Effect on Crystal Growth of Copper Oxide. *Langmuir* **2001**, *17* (5), 1406–1410.

(38)   Pendashteh, A.; Mousavi, M. F.; Rahmanifar, M. S. Fabrication of Anchored Copper Oxide Nanoparticles on Graphene Oxide Nanosheets via an Electrostatic Coprecipitation and Its Application as Supercapacitor. *Electrochimica Acta* **2013**, *88*, 347–357.

(39)   Lu, Y.; Liu, X.; Qiu, K.; Cheng, J.; Wang, W.; Yan, H.; Tang, C.; Kim, J.-K.; Luo, Y. Facile Synthesis of Graphene-Like Copper Oxide Nanofilms with Enhanced Electrochemical and Photocatalytic Properties in Energy and Environmental Applications. *ACS Appl. Mater. Interfaces* **2015**, *7* (18), 9682–9690.

(40)   Li, A.; Song, H.; Wan, W.; Zhou, J.; Chen, X. Copper Oxide Nanowire Arrays Synthesized by In-Situ Thermal Oxidation as an Anode Material for Lithium-Ion Batteries. *Electrochimica Acta* **2014**, *132*, 42–48.

(41)   Rubilar, O.; Rai, M.; Tortella, G.; Diez, M. C.; Seabra, A. B.; Durán, N. Biogenic Nanoparticles: Copper, Copper Oxides, Copper Sulphides, Complex Copper Nanostructures and Their Applications. *Biotechnol Lett* **2013**, *35* (9), 1365–1375.

(42)   Sun, S.; Sun, Y.; Chen, A.; Zhang, X.; Yang, Z. Nanoporous Copper Oxide Ribbon Assembly of Free-Standing Nanoneedles as Biosensors for Glucose. *Analyst* **2015**, *140* (15), 5205–5215.

(43)   Shinde, S. K.; Dubal, D. P.; Ghodake, G. S.; Fulari, V. J. Hierarchical 3D-Flower-like CuO Nanostructure on Copper Foil for Supercapacitors. *RSC Adv.* **2014**, *5* (6), 4443–4447.

(44)   Pal, J.; Ganguly, M.; Mondal, C.; Roy, A.; Negishi, Y.; Pal, T. Crystal-Plane-Dependent Etching of Cuprous Oxide Nanoparticles of Varied Shapes and Their Application in Visible Light Photocatalysis. *J. Phys. Chem. C* **2013**, *117* (46), 24640–24653.

(45)   Lu, Y.; Liu, X.; Qiu, K.; Cheng, J.; Wang, W.; Yan, H.; Tang, C.; Kim, J.-K.; Luo, Y. Facile Synthesis of Graphene-Like Copper Oxide Nanofilms with Enhanced Electrochemical and Photocatalytic Properties in Energy and Environmental Applications. *ACS Appl. Mater. Interfaces* **2015**, *7* (18), 9682–9690.

(46)   Khullar, S.; Thakur, S.; Mandal, S. K. Synthesis and Structural Characterization of Zn(II) and Cd(II) Ion Directed Coordination Networks and Their Template-Free Fabrication to Metal Oxide Nanomaterials. *Inorganica Chimica Acta* **2020**, *502*, 119281.

(47)   Thakur, S.; Mandal, S. K. Effect of Dilution in a Hydrothermal Process and Post-Synthetic Annealing on the Tailoring of Hierarchical ZnO Nanostructures. *CrystEngComm* **2020**, *22* (17), 3059–3069.

(48)   Kumar, N.; Khullar, S.; Mandal, S. K. Controlling the Self-Assembly of Homochiral Coordination Architectures of CuII by Substitution in Amino Acid Based Ligands:

Synthesis, Crystal Structures and Physicochemical Properties. *Dalton Trans.* **2015**, *44* (12), 5672–5687.

(49)   Taghavi Fardood, S.; Ramazani, A. Green Synthesis and Characterization of Copper Oxide Nanoparticles Using Coffee Powder Extract. *Journal of Nanostructures* **2016**, *6* (2), 167–171.

(50)   Sadollahkhani, A.; Hussain Ibupoto, Z.; Elhag, S.; Nur, O.; Willander, M. Photocatalytic Properties of Different Morphologies of CuO for the Degradation of Congo Red Organic Dye. *Ceramics International* **2014**, *40* (7, Part B), 11311–11317.

(51)   Sundar, S.; Venkatachalam, G.; Kwon, S. J. Biosynthesis of Copper Oxide (CuO) Nanowires and Their Use for the Electrochemical Sensing of Dopamine. *Nanomaterials* **2018**.

(52)   Myrach, P.; Nilius, N.; Levchenko, S. V.; Gonchar, A.; Risse, T.; Dinse, K.-P.; Boatner, L. A.; Frandsen, W.; Horn, R.; Freund, H.-J.; Schlögl, R.; Scheffler, M. Temperature-Dependent Morphology, Magnetic and Optical Properties of Li-Doped MgO. *ChemCatChem* **2010**, *2* (7), 854–862.

(53)   Hu, J.; Jiang, Y.; Meng, X.; Lee, C.-S.; Lee, S.-T. Temperature-Dependent Growth of Germanium Oxide and Silicon Oxide Based Nanostructures, Aligned Silicon Oxide Nanowire Assemblies, and Silicon Oxide Microtubes. *Small* **2005**, *1* (4), 429–438.

(54)   Cheng, Q.; Ostrikov, K. (Ken). Temperature-Dependent Growth Mechanisms of Low-Dimensional ZnO Nanostructures. *CrystEngComm* **2011**, *13* (10), 3455–3461.

(55)   Zhou, G.; Yang, J. C. Temperature Effect on the Cu_2O Oxide Morphology Created by Oxidation of Cu(0 0 1) as Investigated by in Situ UHV TEM. *Applied Surface Science* **2003**, *210* (3), 165–170.

(56)   Guo, B.; Košiček, M.; Fu, J.; Qu, Y.; Lin, G.; Baranov, O.; Zavašnik, J.; Cheng, Q.; Ostrikov, K. (Ken); Cvelbar, U. Single-Crystalline Metal Oxide Nanostructures Synthesized by Plasma-Enhanced Thermal Oxidation. *Nanomaterials (Basel)* **2019**, *9* (10).

(57)   Rakhi, R. B.; Chen, W.; Cha, D.; Alshareef, H. N. Influence of Calcination Temperature on the Morphology and Energy Storage Properties of Cobalt Oxide Nanostructures Directly Grown over Carbon Cloth Substrates. *Mater Renew Sustain Energy* **2013**, *2* (3–4).

(58)   Venu Gopal, V. R.; Kamila, S. Effect of Temperature on the Morphology of ZnO Nanoparticles: A Comparative Study. *Appl Nanosci* **2017**, *7* (3), 75–82.

(59)   Shyjumon, I.; Gopinadhan, M.; Ivanova, O.; Quaas, M.; Wulff, H.; Helm, C. A.; Hippler, R. Structural Deformation, Melting Point and Lattice Parameter Studies of Size Selected Silver Clusters. *Eur. Phys. J. D* **2006**, *37* (3), 409–415.

(60)   Buffat, Ph.; Borel, J.-P. Size Effect on the Melting Temperature of Gold Particles. *Physical Review A* **1976**, *13*, 2287–2298.

(61)   Sylvestre, J.-P.; Poulin, S.; Kabashin, A. V.; Sacher, E.; Meunier, M.; Luong, J. H. T. Surface Chemistry of Gold Nanoparticles Produced by Laser Ablation in Aqueous Media. *J. Phys. Chem. B* **2004**, *108* (43), 16864–16869.

(62)   Chakma, S.; Moholkar, V. S. Sonochemical Synthesis of Mesoporous $ZrFe_2O_5$ and Its Application for Degradation of Recalcitrant Pollutants. *RSC Adv.* **2015**, *5* (66), 53529–53542.

(63)   Müller, C.; Nijkamp, M. G.; Vogt, D. Continuous Homogeneous Catalysis. *European Journal of Inorganic Chemistry* **2005**, *2005* (20), 4011–4021.

(64)   Mizuno, N.; Misono, M. Heterogeneous Catalysis. *Chem. Rev.* **1998**, *98* (1), 199–218.

(65) Corma, A. Heterogeneous Catalysis: Understanding for Designing, and Designing for Applications. *Angewandte Chemie International Edition* **2016**, *55* (21), 6112–6113.

(66) Copéret, C.; Chabanas, M.; Saint- Arroman, R. P.; Basset, J.-M. Homogeneous and Heterogeneous Catalysis: Bridging the Gap through Surface Organometallic Chemistry. *Angewandte Chemie International Edition* **2003**, *42* (2), 156–181.

(67) Liu, Z.; Ganguly, R.; Vidović, D. Pursuing the Active Species in an Aluminium-Based Lewis Acid System for Catalytic Diels–Alder Cycloadditions. *Dalton Trans.* **2017**, *46* (3), 753–759.

(68) Yin, Q.; Kemper, S.; Klare, H. F. T.; Oestreich, M. Boron Lewis Acid-Catalyzed Hydroboration of Alkenes with Pinacolborane: BArF$_3$ Does What B(C$_6$F$_5$)$_3$ Cannot Do! *Chemistry – A European Journal* **2016**, *22* (39), 13840–13844.

(69) Scott, D. J.; Phillips, N. A.; Sapsford, J. S.; Deacy, A. C.; Fuchter, M. J.; Ashley, A. E. Versatile Catalytic Hydrogenation Using A Simple Tin(IV) Lewis Acid. *Angewandte Chemie International Edition* **2016**, *55* (47), 14738–14742.

(70) Evans, D. A.; Miller, S. J.; Lectka, T.; von Matt, P. Chiral Bis(Oxazoline)Copper(II) Complexes as Lewis Acid Catalysts for the Enantioselective Diels−Alder Reaction. *J. Am. Chem. Soc.* **1999**, *121* (33), 7559–7573.

(71) Ravasio, N.; Zaccheria, F.; Gervasini, A.; Messi, C. A New, Fe Based, Heterogeneous Lewis Acid: Selective Isomerization of α-Pinene Oxide. *Catalysis Communications* **2008**, *9* (6), 1125–1127.

(72) Kumar, P.; Pandey, R. K.; Bodas, M. S.; Dagade, S. P.; Dongare, M. K.; Ramaswamy, A. V. Acylation of Alcohols, Thiols and Amines with Carboxylic Acids Catalyzed by Yttria–Zirconia-Based Lewis Acid. *Journal of Molecular Catalysis A: Chemical* **2002**, *181* (1), 207–213.

(73) Hashimoto, T.; Omote, M.; Kano, T.; Maruoka, K. Asymmetric 1,3-Dipolar Cycloadditions of Nitrones and Methacrolein Catalyzed by Chiral Bis-Titanium Lewis Acid: A Dramatic Effect of N-Substituent on Nitrone. *Org. Lett.* **2007**, *9* (23), 4805–4808.

(74) Xia, Y.; Xiong, Y.; Lim, B.; Skrabalak, S. E. Shape-Controlled Synthesis of Metal Nanocrystals: Simple Chemistry Meets Complex Physics? *Angewandte Chemie International Edition* **2009**, *48* (1), 60–103.

(75) Wang, J. L.; Ando, R. A.; Camargo, P. H. C. Investigating the Plasmon-Mediated Catalytic Activity of AgAu Nanoparticles as a Function of Composition: Are Two Metals Better than One? *ACS Catal.* **2014**, *4* (11), 3815–3819.

(76) Jia, C.-J.; Schüth, F. Colloidal Metal Nanoparticles as a Component of Designed Catalyst. *Phys. Chem. Chem. Phys.* **2011**, *13* (7), 2457–2487.

(77) Dallavalle, F.; Folesani, G.; Marchelli, R.; Galaverna, G. Stereoselective Formation of Ternary Copper(II) Complexes of (S)-Amino-Acid Amides and (R)- or (S)-Amino Acids in Aqueous Solution. *Helvetica Chimica Acta* **1994**, *77* (6), 1623–1630.

(78) Sa, B.; Hj, K.; Mj, K.; A, R. Planetary Organic Chemistry and the Origins of Biomolecules. *Cold Spring Harb Perspect Biol* **2010**, *2* (7), a003467–a003467.

(79) Qiu, C.; Yu, H.; Qiu, C.; Li, F.; Suo, T.; Wang, C.; Bie, S.; Li, Z. Metal-Free Halogenation of N-Substituted Enaminoesters and Enaminones: A Facile Access to Functionalized α,α-Dihaloimines. *Synthesis* **2020**, *52* (08), 1301–1314.

(80) Park, J.; Feng, D.; Yuan, S.; Zhou, H.-C. Photochromic Metal–Organic Frameworks: Reversible Control of Singlet Oxygen Generation. *Angewandte Chemie International Edition* **2015**, *54* (2), 430–435.

(81) Cleaves, H. J.; Chalmers, J. H.; Lazcano, A.; Miller, S. L.; Bada, J. L. A Reassessment of Prebiotic Organic Synthesis in Neutral Planetary Atmospheres. *Orig Life Evol Biosph* **2008**, *38* (2), 105–115.

(82) Herrera, R. P.; Marqués-López, E. *Multicomponent Reactions: Concepts and Applications for Design and Synthesis*; John Wiley & Sons, 2015.